To the Graduate Council:

I am submitting herewith a thesis written by Joshua Chamot entitled "Modal Mineralogy of the H-group Chondrites: Progressive Effects of Metamorphism." I have examined the final copy of this thesis for form and content and recommended that it be accepted in partial fulfillment of the requirement for the degree of Master of Science, with a major in Geology.

Harry Y. McSween, Jr., Major Professor

We have read this thesis
And recommend its acceptance:

Accepted for Council:

Interim Vice Provost and
Dean of the Graduate School

Modal Mineralogy of the H-group Chondrites: Progressive Effects of Metamorphism

A Thesis
Presented for the
Master of Science Degree
The University of Tennessee

Joshua A. Chamot
December, 2000

Dedication

As the culmination of the first stage of my academic career, this thesis is dedicated to the fine educators, academic and otherwise, from day one to the present, within the classroom and without, even when they least expected it, who guided and supported me to this end.

Q.E.D.

This research is equally dedicated to my mother and father, Judith and Dennis Chamot, my brother Jonathan, my extended family, my friends, and several devoted creatures great and small for their continuing support throughout its completion, without which I would not have succeeded.

Acknowledgements

This thesis would not have reached completion without the advice and guidance of my advisor, Hap McSween, who encouraged me to make this a document of which I would be proud and for editing it with an eye for good writing; the endless support of Heather Gastineau who guided me through every stage of the research with inhuman patience; Larry Taylor for guidance and advice, and instruction on how to get data that could withstand the rigors of the scientific method; Allan Patchen for overseeing and directing my time on the electron microprobe and answering my myriad and oft repeated questions; Dan Britt and Ted Labotka for answering random questions at random times; Mike Wyatt for guiding me through the intricacies of Microsoft products; and Marvin Bennet for providing necessary computer programs, help with meteorite shock classification, advice, guidance, an open ear, and the millions of other favors even on short notice.

Abstract

For several ordinary chondrite mineral phases, CIPW normative abundances are noticeably higher than modal abundances The discrepancy may result in part from the failure of the CIPW calculation to account for the Al and Ca enriched mesostasis phase found in ordinary chondrites.

The discrepancy is relatively uniform among the analyzed chondrites and may not significantly affect certain petrologic trends that were uncovered using normative calculations. Specifically, the norm trend suggesting oxidation with increasing metamorphism (McSween and Labotka, 1993) is supported by Fe enrichment in H chondrite olivine and low-Ca pyroxene, and an increase in modal H chondrite olivine abundance.

The chemical and mineralogic data for H5 and H6 values commonly overlap, possibly a result of our small sample size or the misclassification of one or more chondrites. However, overlap also appears in L and LL chondrite data (e g., Gastineau, 2000; McSween and Labotka, 1993) and may actually be the result of the gradational nature of ordinary chondrite metamorphism. Petrologic trends may be more apparent from analyses of a wider range of petrologic types, as opposed to observations of adjacent petrologic types.

Plagioclase abundance did not appear to increase from type 5 to type 6 in our meteorites, suggesting that plagioclase had crystallized completely by type 5. While mesostasis remains in type 6 chondrites, the plagioclase component appears to have devitrified during type 5 metamorphism. Geothermometers that

rely on plagioclase crystallizing during type 6 metamorphism may not be valid However, the leading alternative — the pyroxene geothermometer — has its own pitfalls when applied to ordinary chondrites, including the possibility that high-Ca pyroxene may not have been completely equilibrated.

The high-Fe chondrite Burnwell, while unique among the known ordinary chondrites, may not represent a specimen from a previously unsampled parent body. Many of the trends in our study indicate that Burnwell petrologic characteristics lie outside of the present range for H chondrites. However, in several trends, the gap between H chondrite and Burnwell values is smaller than the gaps between other ordinary chondrite petrologic groups. Hopefully, additional low-FeO falls will be collected, and classifications can be determined in light of petrologic types other than type 4.

Because normative and modal data are not identical, previous applications of normative data to asteroid spectroscopy should be revisited While trends and overall conclusions probably will not need adjustment, the spectral data sets may need to be re-evaluated Since overall conclusions should persist in the light of new modal data, we still believe that asteroid 6 Hebe represents the best candidate for an H chondrite parent body.

Table of Contents

List of Tables

List of Figures

I. Introduction

Until the first asteroid samples are collected *in situ*, researchers must rely on meteorites and spectral observations to study the thermal histories of meteorite parent bodies. Because chondrite mineral modes are difficult to determine by optical point counts, many studies rely upon normative minerals calculated from high-quality bulk chemical analyses (e.g., McSween et al., 1991). As a result, several subsequent studies have correlated asteroid spectra to normative ordinary chondrite mineral abundances (e.g , Gaffey and Gilbert, 1998).

The CIPW norm calculation was devised for terrestrial igneous rocks and may not reveal the true mineral assemblages of chondritic meteorites. Therefore, the mineralogic trends researchers have observed in chondrites and inferred from asteroid spectra may potentially be artifacts of the normative calculations, not the properties of the meteorites or their parent bodies. In light of new technologies that enable automated point counting (i.e., modal analyses) with an electron microprobe, normative trends can now be confirmed with modal mineral data.

The H chondrites comprise the largest ordinary chondrite group, and the conditions and timing of their parent body's metamorphism are especially well characterized. As a result, the H chondrites are commonly used as constraints for asteroid thermal modeling. Gastineau (2000) analyzed L and LL chondrites and found significant discrepancies between normative and modal mineral abundances. The present study expands on her research by determining if a similar discrepancy exists in H chondrites.

In the current study, we directly compare normative and modal mineral abundances, and we test petrologic trends that have been suggested using normative data sets. The principal test follows the hypothesis of McSween and Labotka (1993) that oxidation accompanied the metamorphism of ordinary chondrites, producing olivine at the expense of pyroxene and Fe metal. Additionally, we look at how progressive metamorphism within ordinary chondrites is reflected by the devitrification of glass to form plagioclase and how the process relates to chondrite geothermometery. Applying our conclusions, we explore the implications of the new modal data for asteroid spectroscopy — particularly for a proposed H chondrite parent body, asteroid 6 Hebe (Gaffey and Gilbert, 1998) Finally, we compare modal analyses of the extremely Fe-rich chondrite Burnwell to other ordinary chondrites of similar metamorphic grade. Burnwell has been suggested as the first sampling of a new, low-FeO, high bulk Fe chondrite group (Russell et al., 1998), and our analyses will test that conclusion.

The importance of H chondrites

Ordinary chondrites are the most common meteorites among falls and in scientific collections. They are primarily classified on the basis of Fe content, oxidation state, and metamorphic grade. In 1953, Urey and Craig published a system of nomenclature for ordinary chondrites based upon the percent of total Fe in the meteorite and the proportion of oxidized to reduced Fe The ordinary

chondrites they analyzed fell into two groups, H (having high total Fe that is more reduced) and L (having less Fe that is more oxidized). Keil and Fredriksson (1964) modified the classification by establishing the ratio Fe/(Fe+Mg) in the dominant silicate phases as the defining parameter. In a plot of Fe/(Fe+Mg) in olivines versus Fe/(Fe+Mg) in pyroxenes, they found three distinct groups, two of which are identical to the H and L groups of Urey and Craig (1953) and a third that they designated LL — characterized by both low bulk Fe and low total metal.

The H chondrites are the most thoroughly studied ordinary chondrites because they are much more abundant than the LL chondrites and tend to yield clearer petrologic trends than the more severely shocked L chondrites. Because shock metamorphism has not reset their peak temperatures, cooling rates, and chronology, H chondrites have been the basis for several seminal papers on asteroid thermal history (e.g. Miyamoto et al., 1981, Bennett and McSween, 1996; Ghosh and McSween, 2000)

Recent studies suggest that there may also be an H-group extreme — dubbed "low-FeO" (Russell et al., 1998) or "HH" (e g., McSween et al , 1991) chondrite. The majority of low-FeO chondritic material is either terrestrially weathered, is chemically disequilibrated, or occurs as silicate inclusions within IIE iron meteorites However, Russell et al (1998) described the new meteorite Burnwell, which is a low-FeO chondrite and is a relatively equilibrated, unweathered fall. We included Burnwell in our sample set, both to evaluate its modal relationships to the H chondrites and to expand further upon the previous

studies of L and LL chondrites by Gastineau (2000).

The ordinary chondrites are subdivided based upon petrologic differences reflecting degree of metamorphism. The classification ranges from "type 3," which represents a nearly unmetamorphosed chondrite, to "type 6," which represents a further metamorphosed chondrite with more equilibrated mineral phases (Van Schmus and Wood, 1967). There are several criteria for determining the degree of equilibration: homogeneity of silicate mineral compositions, ratio of low-Ca monoclinic pyroxene to orthorhombic pyroxene, absence (at lower metamorphic grade) of well crystallized feldspar, presence (at lower metamorphic grade) of igneous glass within chondrules, compositions of metallic and sulfide minerals, homogenization and coarsening of textures at higher metamorphic grades, and bulk C and H_2O contents (Van Schmus and Wood, 1967)

It is important to note that the metamorphic trends in chondrites are mostly continuous reactions, and the petrologic types are separated by arbitrarily defined petrologic boundaries. As a result, two chondrites assigned to different petrologic types could be similar — for example, an H5 chondrite near the type-5 upper metamorphic extreme could be similar to an H6 chondrite near the type-6 lower metamorphic extreme. From our present research, we suggest that several mineral properties may overlap between H5 and H6 conditions in ordinary chondrites.

Ordinary chondrite metamorphic trends reflecting Fe oxidation

While many researchers have observed a subtle variation in Fe oxidation state between the different petrologic types, researchers have not agreed on whether oxidation or reduction results from progressive metamorphism. Earlier studies relying on siderophile element abundances (Sears and Weeks, 1986) or measured oxygen fugacity (Brett and Sato, 1984) suggest that Fe was reduced with increasing metamorphism. However, relying on averaged normative mineralogical data from McSween et al. (1991), McSween and Labotka (1993) observed that in type 4-6 ordinary chondrites, metallic Fe was oxidized during heating While not yet directly observed in petrographic textures, McSween and Labotka (1993) observed mineralogic evidence for the reaction. Specifically, they found that olivine abundance increased with metamorphic grade at the expense of pyroxene and metal. Their proposed mechanism can be expressed in the following reaction.

$$Fe_{(metal)} + O_{(possibly\ in\ H2O)} + (Mg, Fe)SiO_{3\ (pyroxene)} = (Mg, Fe)_2SiO_{4\ (olivine)}$$

McSween and Labotka (1993) proposed that progressive oxidation was promoted by small amounts of an oxidizing fluid, possibly the byproduct of the heating of ices originally accreted into the parent asteroid. The progressive oxidation in the metamorphic sequence resulted from different degrees of reaction with the oxidizing fluid, possibly due to variations in temperature or the evolution

of the fluid composition as it permeated through the asteroid (McSween and Labotka, 1993).

Our study investigates the Fe oxidation trend and other petrologic variations for H chondrites, trends that Gastineau (2000) confirmed in modal analyses of L and LL chondrites. Foremost, she recognized that while olivine increased with progressive metamorphism, supporting the oxidation trend of McSween and Labotka (1993), the modal olivine/low-Ca pyroxene ratios were offset below the normative ratios. She suggested that the inconsistency may be due to the extremely reduced metal-bearing nature of the rocks. In addition, the Fe-Mg distribution coefficient for olivine and hypersthene applied in CIPW norm calculations is different from the actual partitions in the chondrites (McSween et al., 1991).

Gastineau (2000) also recognized that the molar Fe/Mn and Fe/Mg ratios within olivine, low-Ca pyroxene, and high-Ca pyroxene generally increase from petrologic types 4 to 6, although the trend is unclear for some specimens. The observed trend reflects Fe enrichment within these mineral phases (Goodrich and Delaney, 2000). Gastineau (200) suggested that as metal is oxidized during progressive metamorphism, Fe^{2+} diffuses outwards into chondritic silicates.

From the same plot, Gastineau (2000) recognized that tie lines connecting olivine to low-Ca pyroxene and tie lines connecting high-Ca pyroxene to low-Ca pyroxene are roughly parallel. She suggested that parallel tie lines show that the phases approach equilibrium in terms of Fe/Mn and Fe/Mg, although some

crossing implied disequilibrium in several meteorites. She suggested that the reason for disequilibrium was (1) the gradational boundaries between petrologic types, or (2) re-equilibration during cooling (following peak metamorphism). Gastineau (2000) concluded that for L and LL chondrite mineral modes, metallic Fe, pyroxene, and an oxidizing agent combined to form olivine, following the trend McSween and Labotka (1993) observed in normative minerals.

Plagioclase abundance in the ordinary chondrites

Another key trend in chondrite metamorphism is the conversion of glass to plagioclase as metamorphism progresses. The increase in plagioclase abundance with metamorphism that Gastineau (2000) observed supports earlier studies (e.g. Van Schmus and Wood, 1967); however, she also observed some high-silica phase (possibly glass) within the highly metamorphosed type 6 meteorites. The occurrence of a high-silica phase in type 6 meteorites is contrary to studies that suggest that all glass has devitrified to plagioclase by that point (e.g., Sears et al , 1980)

The Van Schmus and Wood (1967) classification system considers the loss of igneous glass and the development of secondary feldspar to be indicative of increasing petrologic type. Under their classification, igneous glass was scarce by type 4 conditions and absent by type 5, when it was completely converted into feldspar. More recent thermoluminescence studies (e.g., Sears et al., 1980) have shown that some feldspar crystallization persists under type 5 conditions,

although glass is rare. Our research relates plagioclase abundance to petrologic type to determine when glass appears to have completely converted to plagioclase and to determine whether the normative and modal data converge as glass is devitrified, as seen by Gastineau (2000).

In addition to aiding with classification, plagioclase can be used as a chondrite geothermometer. Nakamuta and Motomura (1999) used a sodic plagioclase geothermometer to determine average temperatures for H6, L6, and LL6 chondrites. However, their results for H6 chondrites (725°-742°C) are generally lower than H6 temperatures determined using the Lindsley and Anderson (1983) two-pyroxene geothermometer. Because peak metamorphic temperature is a constraint for asteroid thermal models (e g., Miyamoto et al., 1981; Ghosh and McSween, 2000), it is necessary that researchers determine the accuracy of the different chondrite geothermometers.

Asteroid 6 Hebe: A proposed parent body for H chondrites

Several factors link asteroid 6 Hebe to the parent body for H chondrites, including size, location within the solar system, and most critically, inferred surface composition. Parent body size is determined from internal heating models, ultimately derived from ordinary chondrite peak metamorphic temperatures. Thermal models based on the decay of ^{26}Al (Miyamoto et al., 1981; Bennett and McSween, 1996) indicate that parent asteroids have highly metamorphosed, type 6 chondrite material at their centers and grade outwards to

type 3 chondrite material at their rims. This stratified structure is called the "onion-shell model," in contrast to the "rubble pile" scenario proposed by Scott and Rajan (1981) and others which suggests that smaller bodies underwent various degrees of metamorphism and then accreted into the larger asteroid parent bodies. In addition, rubble piles could result from impact disruption and gravitational re-accretion of a large, onion-shell body (Taylor et al., 1987). Göpel et al. (1994) used U-Pb closure times in chondritic phosphates to confirm that H6 material cooled more slowly (i.e., at greater burial depth) than less equilibrated H chondrite material, supporting the onion-shell model for the original structure of the H chondrite parent body.

In revising the Miyamoto et al. (1981) model with the U-Pb closure times and other data, Bennett and McSween (1996) suggested that the radius of the H chondrite parent body ranged in size between 80km and 95 km. The range matches the radius of asteroid 6 Hebe (Gaffey and Gilbert, 1998). The thermal model of 6 Hebe has since been refined by taking incremental accretion into account (Ghosh and McSween, 2000), but the basic size parameters remain unchanged.

In regards to location within the solar system, 6 Hebe lies close to asteroid belt escape regions needed to supply meteorites to Earth — specifically, near the 3:1 proper motion resonance with Jupiter at 2.50 AU (Wisdom, 1985) and the ν_6 secular resonance (Williams and Faulkner, 1981). According to Williams (1973), a relatively low ejection velocity (280 m/s) can place 6 Hebe ejecta —

presumably the H chondrites — into the secular resonance, and eventually into Earth-crossing orbits, within 10^6 years.

The mineral assemblages on the surface of 6 Hebe also suggest a relationship with the H chondrites. As 6 Hebe rotates, different regions of the asteroid face the Earth at any given moment, and the regions reveal different spectra ("rotational spectra") (Gaffey and Gilbert, 1998). The varied spectra suggest that several mineral assemblages coexist on the surface, implying that an "onion-shell" asteroid has shattered, reassembling into a "rubble pile."

Gaffey and Gilbert (1998) were able to determine the specific mineral assemblages using the techniques of Cloutis et al. (1986). On a plot of mineral reflectance versus wavelength, olivine and orthopyroxene assemblages produce absorption features at 1 μm (Band I) and 2 μm (Band II) (Cloutis et al , 1986) Cloutis et al. (1986) found that the spectral position of the Band I minimum and the ratio of the areas of Band II to Band I reflect the abundance and compositions of the olivine and pyroxene phases. Gaffey and Gilbert (1998) calculated an averaged H chondrite spectra using averaged H4, H5, and H6 olivine and pyroxene norm abundances (from McSween and Labotka, 1993) and spectral observations of several meteorites. They found that the averaged H-chondrite spectra and 6 Hebe rotational spectra are similar.

Gaffey and Gilbert (1998) also compared the normative mineralogic pattern of increasing Fe oxidation with petrologic type observed by McSween and Labotka (1993) to the varied spectra ("rotational spectra") of 6 Hebe (fig. 1). If

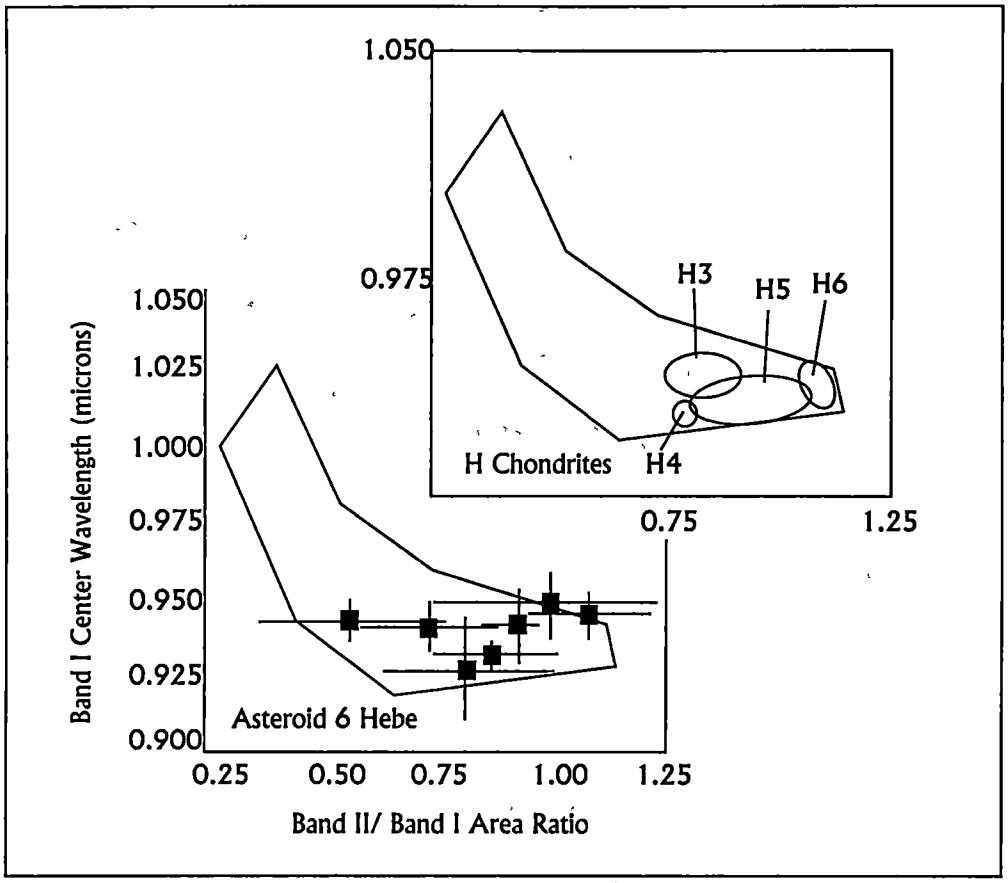

Figure 1: When the spectral characteristics of asteroid 6 Hebe are plotted (specifically the relationship between the center of the Band I absorption feature and the ratio of the areas of the Band I and Band II absorption features), the data points overlap regions defined by H chondrite spectra. Gaffey and Gilbert (1998) suggest that the variety of spectra for H chondrite petrologic types reflect varied mineral assemblages resulting from progressive oxidation (McSween and Labotka, 1993). Because the surface of 6 Hebe overlaps the various petrologic types, Gaffey and Gilbert (1998) believe the asteroid is a rubble pile with a surface that reflects the different H chondrite mineral assemblages. After Gaffey and Gilbert (1998) and McSween (1999).

the norm oxidation trend reflects modal abundances, then the variations in olivine and orthopyroxene proportions on the surface of 6 Hebe may reflect the different oxidation histories of the materials now on the surface of rubble-pile asteroid. Again, because so many of the chondrite to parent body comparisons rely upon normative mineral data, the comparison of H chondrites to the surface mineral assemblage of 6 Hebe may have to be adjusted if the preexisting norm data do not reflect modal values.

Burnwell: a possible "HH" chondrite

The Burnwell meteorite fell on September 4, 1990, smashing through the roof and front porch of a home in Burnwell, Kentucky (Russell et al., 1998). 15.5 x 7 x 5 cm in dimension, Burnwell displays several unusual mineralogic characteristics that distinguish it from other ordinary chondrites. According to Russell et al. (1998), it has lower Fa in olivine (15.8 mol%), lower Fs in orthopyroxene (13.4 mol%), lower Co in kamacite (0.36 wt%), lower bulk FeO (9.43 wt%), lower $\delta^{17}O$ (0.51 ± 0.02 per mil), and higher metallic Fe, Ni, and Co (combined 19.75 wt% from bulk wet chemical analysis) than observed in H chondrites. Our research compares Burnwell modal mineral abundances to norm mineral abundances calculated from the bulk analyses of Russell et al. (1998). In addition, we compare the petrologic properties of H4, L4, and LL4 chondrites to Burnwell — also classified as petrologic type 4 (Russell et al., 1998) — to determine whether the low-FeO chondrite extends these trends.

II. Methods

We analyzed two thin sections for each petrologic type from H4 through H6 and one low-FeO chondrite (Table 1). The chondrites were chosen from a list of those having high-quality bulk chemical analyses by Jarosewich, which McSween et al. (1991) used to calculate norm mineral abundances. Furthermore, we selected meteorite specimens that had relatively large thin section areas and lacked brecciation or large inclusions. We also attempted to obtain chondrites that were spectrally clean — i e , relatively free of terrestrial weathering products such as ferric oxides which alter the visible-near-infrared (VISNIR) spectra. However, only one H chondrite, Allegan (H5), was on the list of spectrally clean meteorites compiled by Gaffey (1999), and we obtained this meteorite. For the rest, we tried to obtain specimens that appeared to be the least weathered under the optical microscope. We also selected meteorites that were not highly shocked. Using the procedure of Stoffler et al. (1991), we analyzed the six ordinary chondrites and Burnwell with a petrologic microscope in both transmitted and reflected light and determined their shock grade. Our shock determinations are compared with several previous determinations in Table 1.

Modal Mineralogy

Few modal data sets exist for the ordinary chondrites (e.g., Bryan and Kullerud, 1975) because of difficulties imposed by their fine-grained textures and problems with distinguishing between olivine and orthopyroxene optically.

Table 1. Meteorites Used in this Study

Chondrite	Name	Brecciation[1]	Shock Grade	Collection
H4[2]	Farmville	No	S3 (S3)[4]	USNM 937-1
H4[2]	Avanhandava	No	S2 (S2)[4]	USNM 6882-1
H5[2]	Ucera	No	S4	USNM 5292-1
H5[2]	Allegan	No	S1	USNM 953-1
H6[2]	Canon City	No	S1	USNM 5733-1
H5[2]/H6[3]	Chiang Khan	No	S3	USNM 6263-1
Low-FeO type 4[5]	Burnwell	Possible[5]	S4 (S4)[5]	USNM 6847-2

1 – Britt and Pieters (1991)
2 – Grady (2000)
3 – Clarke (1982)
4 – Stoffler et al. (1991)
5 – Russell et al. (1998)

However, with an electron microprobe we can now analyze thousands of points and identify grains that are only a few microns in size. Composition maps of each meteorite sample were made using the University of Tennesee's Cameca SX-50 electron microprobe, with each map consisting of between 208,886 (Allegan) to 583,282 (Burnwell) points depending upon thin section size. To compile the point counts, we first determined approximate compositions of mineral phases using the Oxford Instruments (LINK) Model eXL II energy-dispersive spectrometer (EDS). We then made modal composition maps using the EDS and the Oxford software *Feature Scan*

Feature Scan is a semiquantitative technique, with an estimated precision of ~10% of the amount present (Taylor et al., 1996). As a spot is analyzed, *Feature Scan* compares the chemistry of the analysis to a user-defined list of possible mineral candidates, with certain characteristic element abundances serving as defining parameters (Table 2 in Appendix 5). Cracks, overlapping phases, or phases not included in the list are delegated to the "unclassified" bin. As *Feature Scan* progresses, an EDS spectrum is acquired at every 4^{th} pixel (each pixel 4.8 μm). The conditions for the acquisition of X-ray data by the EDS were 20 kV excitation potential, 3nA beam current, and a 60 msec. counting time. The program then tabulates the modal abundance of each mineral.

Because the modal analyses provided by *Feature Scan* are in area percent, we used the procedure of Gastineau (2000) to convert area percent into weight per cent. The conversion requires density values for the various phases. To determine

an olivine density for each meteorite (see Appendix 1), % Fa was calculated from the quantitative chemical analyses and the value was applied to a standard graph of specific gravity vs. mol. % Fa (Deer, Howie, and Zussman 1998). Similarly, to determine a low-Ca pyroxene density for each meteorite (see Appendix 1), we calculated % En from the quantitative analyses and applied the value to a standard graph of specific gravity vs. mol. % En. For analytical consistency, and because the remaining mineral phases are not as varied among chondrite groups, all other densities were taken from Gastineau (2000).

Chemical Analyses

Feature Scan does not give an exact chemical composition. Therefore, it was necessary to perform quantitative chemical analyses to determine the compositions of principal minerals — olivine, low-Ca pyroxene, and high-Ca pyroxene. Using a beam voltage of 15 kV, a beam current of 30 nA, and a beam size of 1 μm, we collected quantitative point analyses of olivine and pyroxene grains using the Cameca electron microprobe Appropriate natural and synthetic standards were used. Matrix corrections were based on ZAF procedures incorporated in the Cameca software. For the H5 and H6 chondrites, we analyzed 3 cores and 3 rims for each grain of olivine and low-Ca pyroxene, and 4 grains of each mineral per meteorite (Appendices 2 and 3). For H4 chondrites and Burnwell, we analyzed twice as many grains because the meteorites are less equilibrated. For high-Ca pyroxene, the grains were too small (most were less

than 10 μm in diameter) to analyze a different core and rim region. Therefore, we analyzed 24 individual high-Ca pyroxene grains per H5 and H6 chondrite and 48 grains per H4 chondrite (and Burnwell) (Appendix 4). The need for many analyses was justified by the relatively wide range of composition for each meteorite phase.

III. Results

Petrologic trends for the H4-H6 chondrites

There are significant, yet generally parallel, differences between the normative and modal trends in all analyses (Table 3). The ratio of olivine/low-Ca pyroxene (low-Ca pyroxene is orthopyroxene + pigeonite) increased with metamorphic grade in both normative and modal data sets (fig. 2). While the trend appears to support the oxidation trend of McSween and Labotka (1993), H5 values are greater than H6 values. In addition, error bars for all three petrologic types overlap. In an attempt to clarify the data, we plotted each mineral phase separately (fig. 3).

Olivine modes generally increase with progressive metamorphism (fig. 3), but the H5 chondrites have a higher average abundance than the H6 chondrites. In low-Ca pyroxene, the H6 chondrites have the highest average modal abundance, yet the H4 chondrites are more enriched than the H5. The normative mineral trend is more difficult to discern because of the wide spread in values between the two H5 chondrites (fig. 2).

Plagioclase consistently increases in concentration from H4 to H6, though as in other trends, there is significant overlap between H5 and H6 values (fig. 4). In contrast to the observations of L and LL chondrites by Gastineau (2000), the modal and normative trends do not converge in type 6 H chondrites. The trend for high-Ca pyroxene concentration is similar to the trend for plagioclase, except the normative and modal trends more closely parallel each other (fig. 5).

Table 3: Mode and Norm Abundances in H chondrites and Burnwell

Mode (without unclassified)	Canon City	Chiang Khan	Ucera	Allegan	Farmville	Avanhandava	Burnwell
Si- and Al-rich glassy mesostasis	2 04	3 02	2 58	3 09	4 40	3 98	5 12
K-rich glassy mesostasis	0 21	0 22	0 40	0 26	0 46	0 27	0 36
phosphate	0 54	0 56	0 47	0 48	0 48	0 51	0 45
ilmenite	0 01	0 03	0 03	0 06	0 01	0 00	0 00
chromite	0 92	1 05	1 25	1 12	1 02	0 91	0 87
kamacite	16 3	14 5	13 6	13 1	15 5	15 5	16 1
taenite	1 34	1 13	1 89	1 23	1 38	1 30	1 03
FeS	5 79	6 52	7.73	7 10	7 61	7 47	7 23
pigeonite	1 30	1 77	1 87	1 83	3 42	2 07	5 76
high-Ca pyroxene	3 19	3 05	3 25	3 20	1 97	2 68	1 97
plagioclase	6 13	5 79	5 78	6 00	4 04	4 65	2 84
Low-Ca pyroxene	30 9	30 1	29 2	30 0	29 9	30 8	32 3
olivine	31 3	32.3	31 9	33 0	29 8	29 9	25 9
Unclassified (in area%)	5 70	6 49	5.44	9.35	8 20	9 29	8 05
Norm	H chondrite norm from McSween et al. (1991), Burnwell norm calculated using procedure of McSween et al. (1991)						
Si- and Al-rich glassy mesostasis	n/a	n/a	n/a	n/a	n/a	n/a	n/a
K-rich glassy mesostasis	0 47	0 48	0 53	0 53	0 54	0 53	0 54
phosphate	0 71	0 57	0 62	0 64	0 62	0 62	0 64
ilmenite	0 26	0 25	0 21	0 19	0 21	0 23	0 19
chromite	0 79	0 74	0 77	0 80	0 73	0 71	0 81
kamacite	18 8	18 0	16 5	19 8	18 5	18 2	19 7
taenite	n/a	n/a	n/a	n/a	n/a	n/a	n/a
FeS	5 61	5 22	6 00	5 54	5 00	5 48	3 64
pigeonite	n/a	n/a	n/a	n/a	n/a	n/a	n/a
high-Ca pyroxene	4 53	4 07	4 34	4 14	3 83	3 76	3 39
plagioclase	9 21	9 71	8 99	8 44	8 72	8 65	8 97
Low-Ca pyroxene	25 4	26 4	26 4	29 0	28 6	28 4	26 9
olivine	34 1	34 6	35 6	30 9	33 3	33 4	35 2
cobalt	n/a	n/a	n/a	n/a	n/a	n/a	0 08

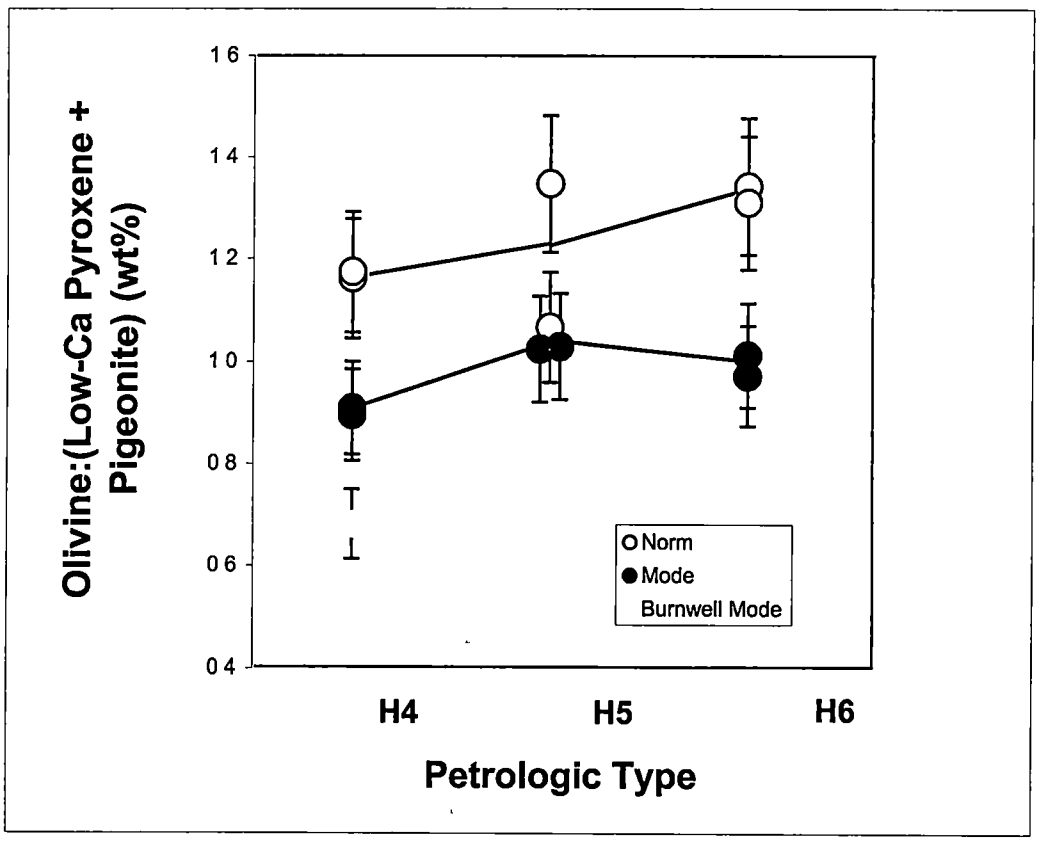

Figure 2: The above diagram shows that the H4 chondrites contain less olivine – with respect to low-Ca pyroxene – than the H6 chondrites. In light of the hypothesis of McSween and Labotka (1993), the trend suggests that Fe metal oxidizes during chondrite metamorphism, because olivine increases at the expense of pyroxene and Fe metal. However, there is an overlap between the H5 and H6 data. Standard deviation is 10% relative to the ratio value.

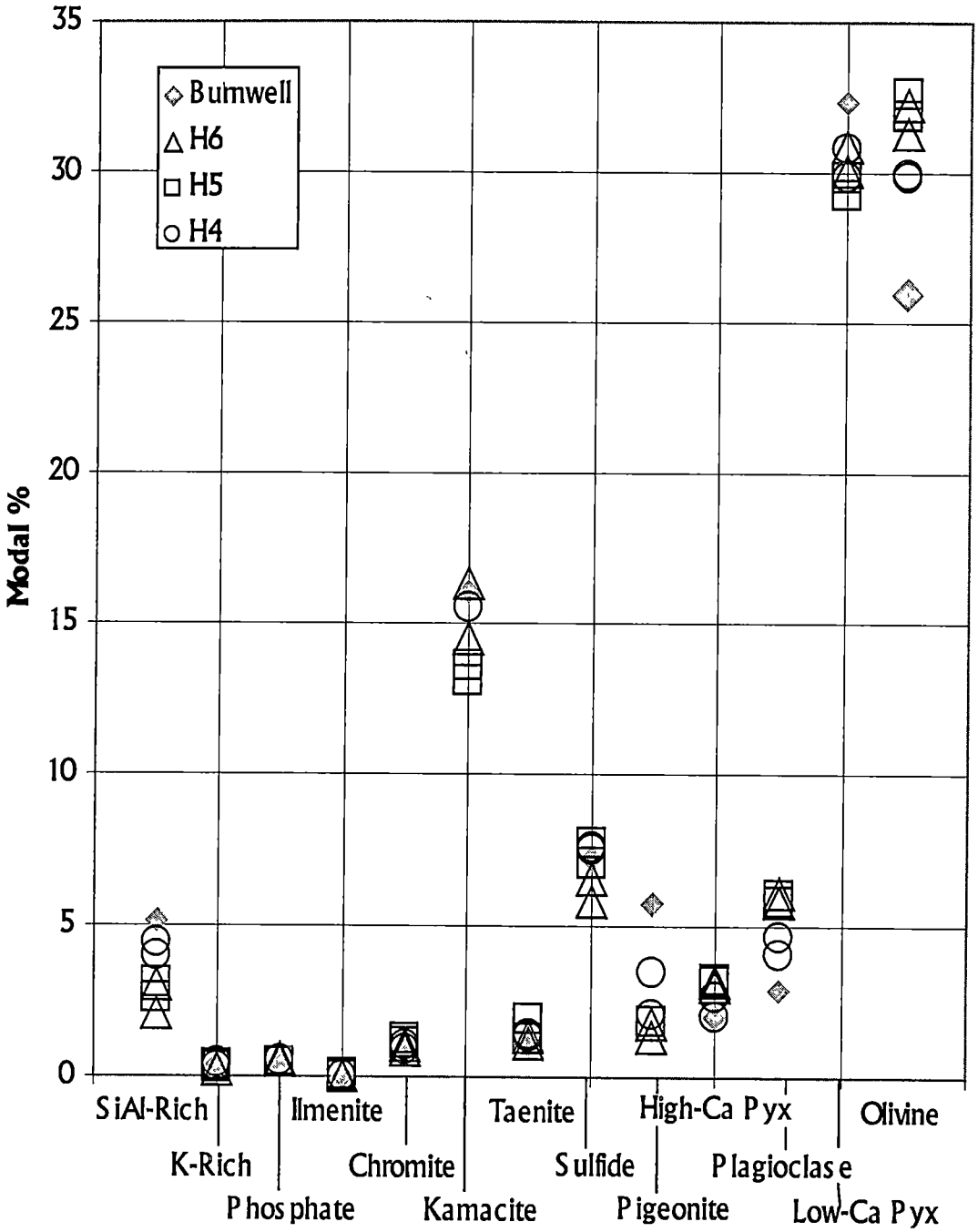

Figure 3: There exists an overlap between H5 and H6 modal abundances, particularly for the SiAl-rich phase, pigeonite, high-Ca pyroxene, the plagioclase phase, and olivine In addition, olivine appears to increase in abundance with metamorphism, as does high-Ca pyroxene, while pigeonite and the SiAl-rich phase appear to decrease.

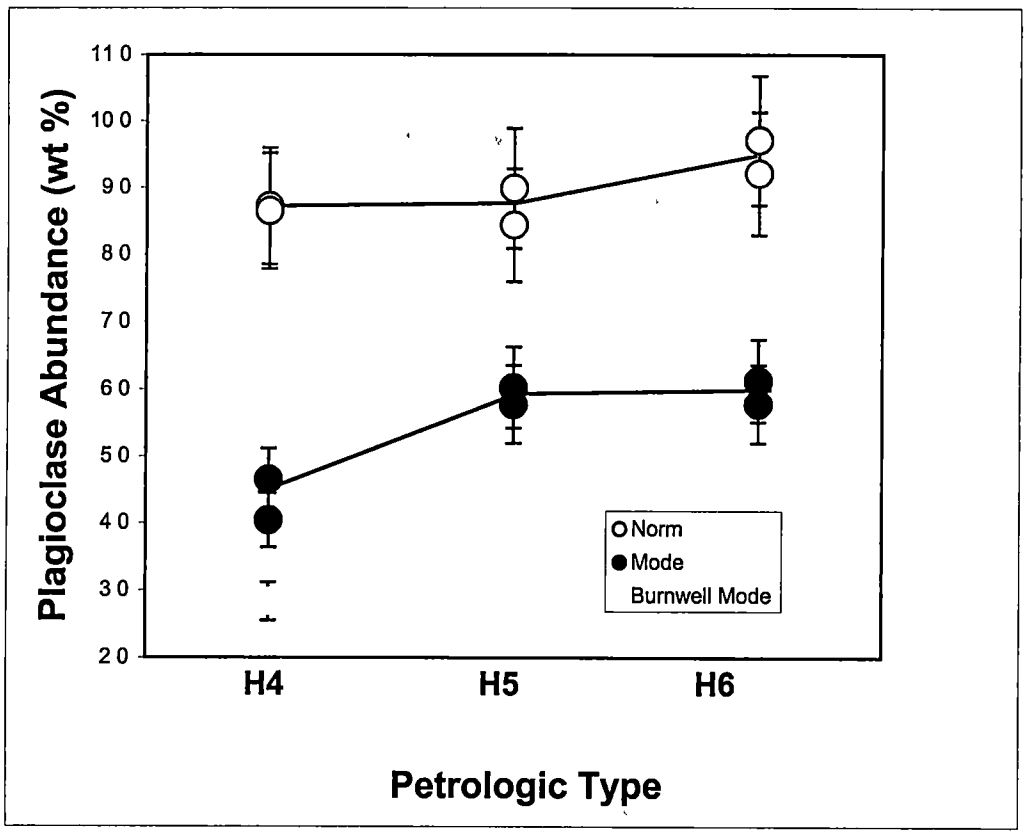

Figure 4: Plagioclase concentrations increase with progressive metamorphism. Because the H5 and H6 values overlap, no new plagioclase appears to form after H6 conditions. The modal and normative data do not converge at H6 as they do for the L and LL chondrites in Gastineau (2000). Standard deviation is 10% relative.

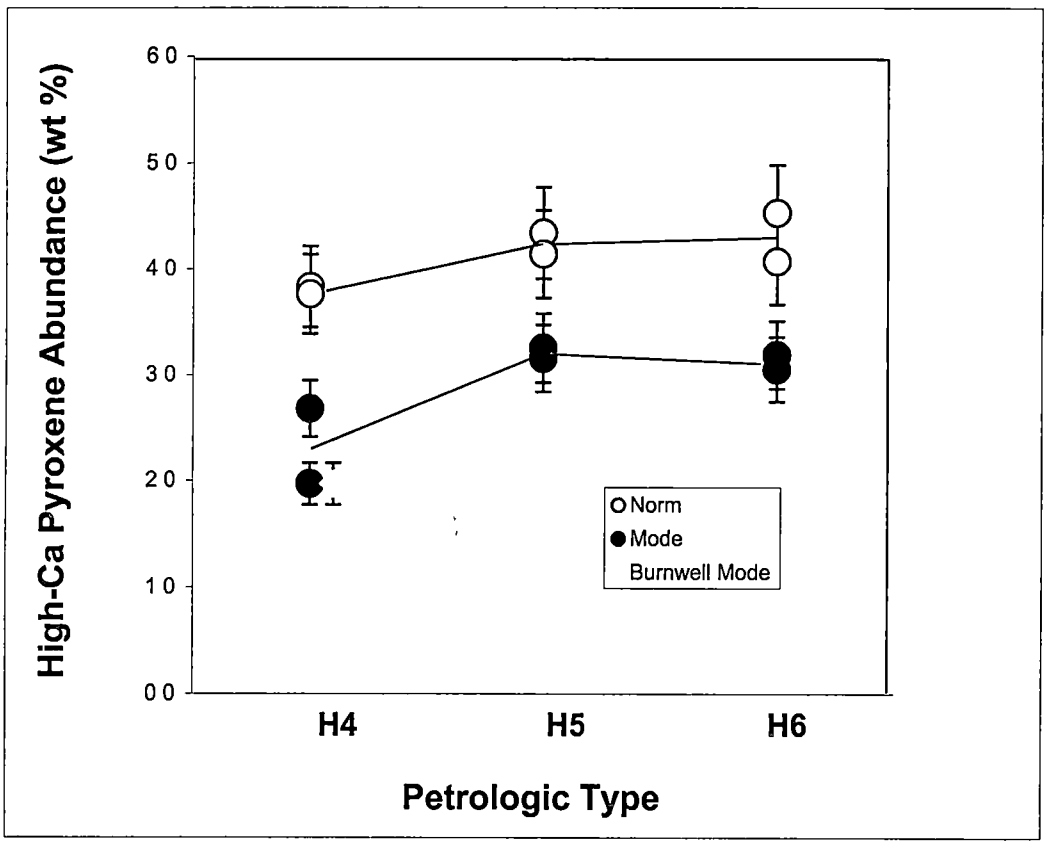

Figure 5: High-Ca pyroxene abundance increases from H4 to H6, with H5 and H6 values overlapping. The modal and normative data do not converge at H6 as they do for L and LL chondrites in Gastineau (2000). Standard deviation is 10% relative.

Chemical analyses of mineral phases

Goodrich and Delaney (2000) analyzed Fe-Mg-Mn relations between different meteorite groups by plotting bulk molar Fe/Mn ratio versus bulk molar Fe/Mg ratio. Gastineau (2000) plotted the same ratios for olivine, low-Ca pyroxene, and high-Ca pyroxene analyses from type 4-6 L and LL chondrites to determine Fe-Mg-Mn relations between these meteorite groups She found that Fe enrichment could be seen with increasing metamorphism in L chondrite olivine and low-Ca pyroxene, and in LL chondrite high-Ca pyroxene. For H chondrites, the concentration of Fe generally increases from petrologic type 4 to type 6, in both our data and data from earlier studies (e.g., Wang and Rubin, 1987), supporting the hypothesis of oxidation with metamorphism (fig. 6).

Tie lines between the mineral phase data points are generally parallel from low-Ca pyroxene to olivine, but some cross from low-Ca pyroxene to high-Ca pyroxene (fig. 6). The crossing may suggest that the olivine and low-Ca pyroxene reached equilibrium in terms of Fe distribution, whereas high-Ca pyroxene may not

The high-Ca pyroxene dis-equilibrium may be because the mineral failed to reach equilibration temperatures for a significant duration of time. In addition, the high-Ca pyroxene continues to form during metamorphism, so metamorphic histories for grains from the same meteorite may differ.

Plots of minor element concentrations support the observation of Fe enrichment within several phases. In olivine (figs. 7,8) and low-Ca pyroxene,

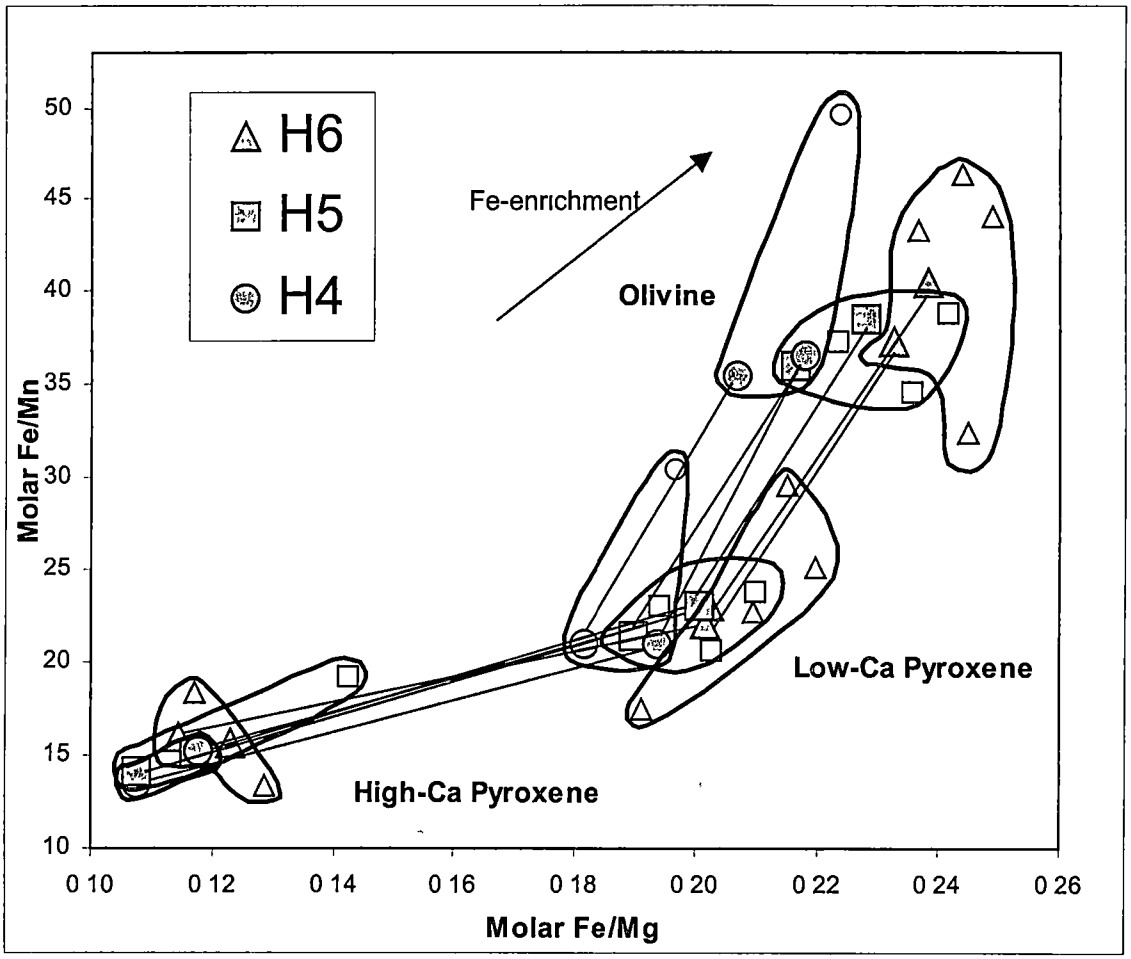

Figure 6: Overall Fe-enrichment occurs from H4 to H6, although there is substantial overlap of values. The trend is most apparent in the olivines and is least apparent in the high-Ca pyroxenes. Tie lines for our data set generally do not cross for low-Ca pyroxene and olivine, suggesting somewhat equilibrated conditions for these phases. Open symbols are previously published microprobe data from. Bryan and Kullerud (1975), Bunch et al. (1972), Fudali and Noonan (1975), Gomes et al. (1977), Jaques et al. (1975), Lange et al. (1974), Wang and Rubin (1987).

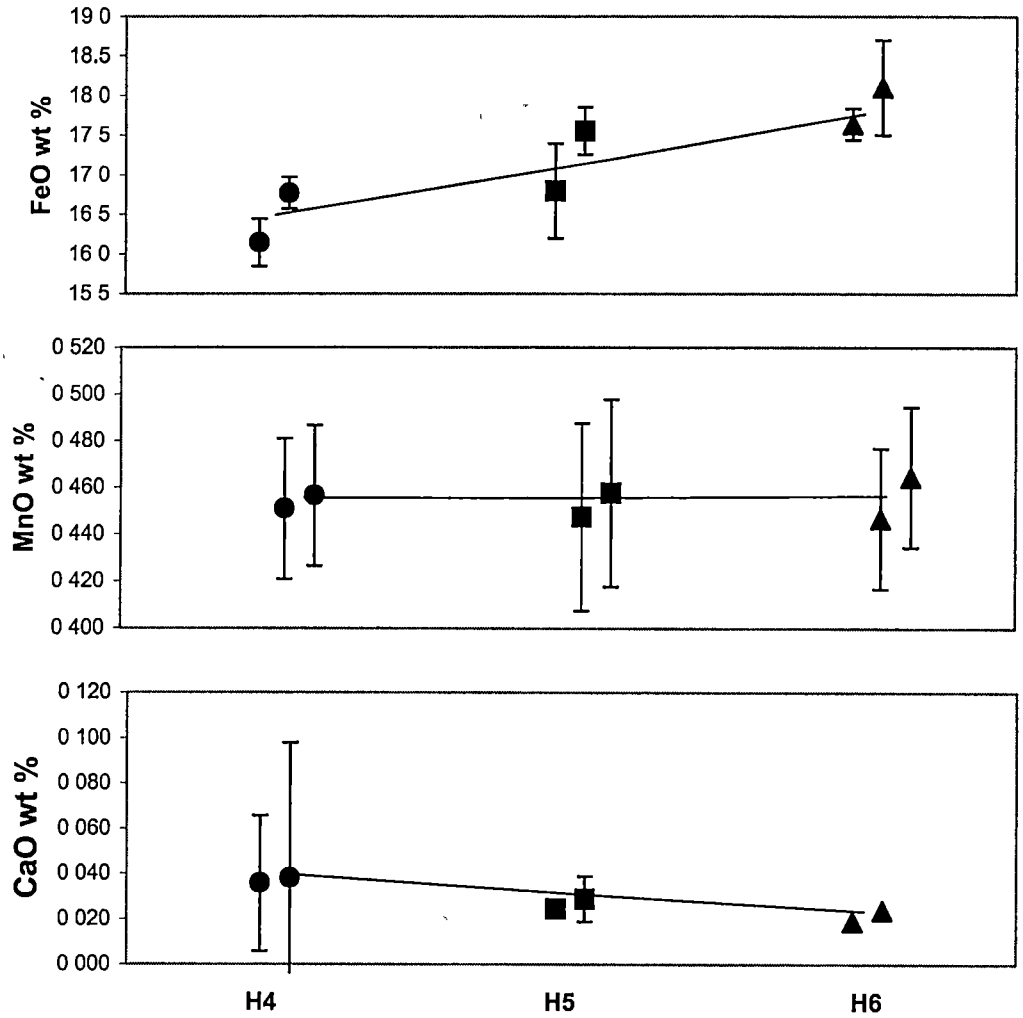

Figure 7: For olivine minor element abundances, FeO increases in abundance from H4 to H6, supporting the hypothesis of Fe oxidation with increasing metamorphism There is no apparent trend in other minor elements Error bars show one standard deviation except for values lying below detection limit, for which error bars are not shown.

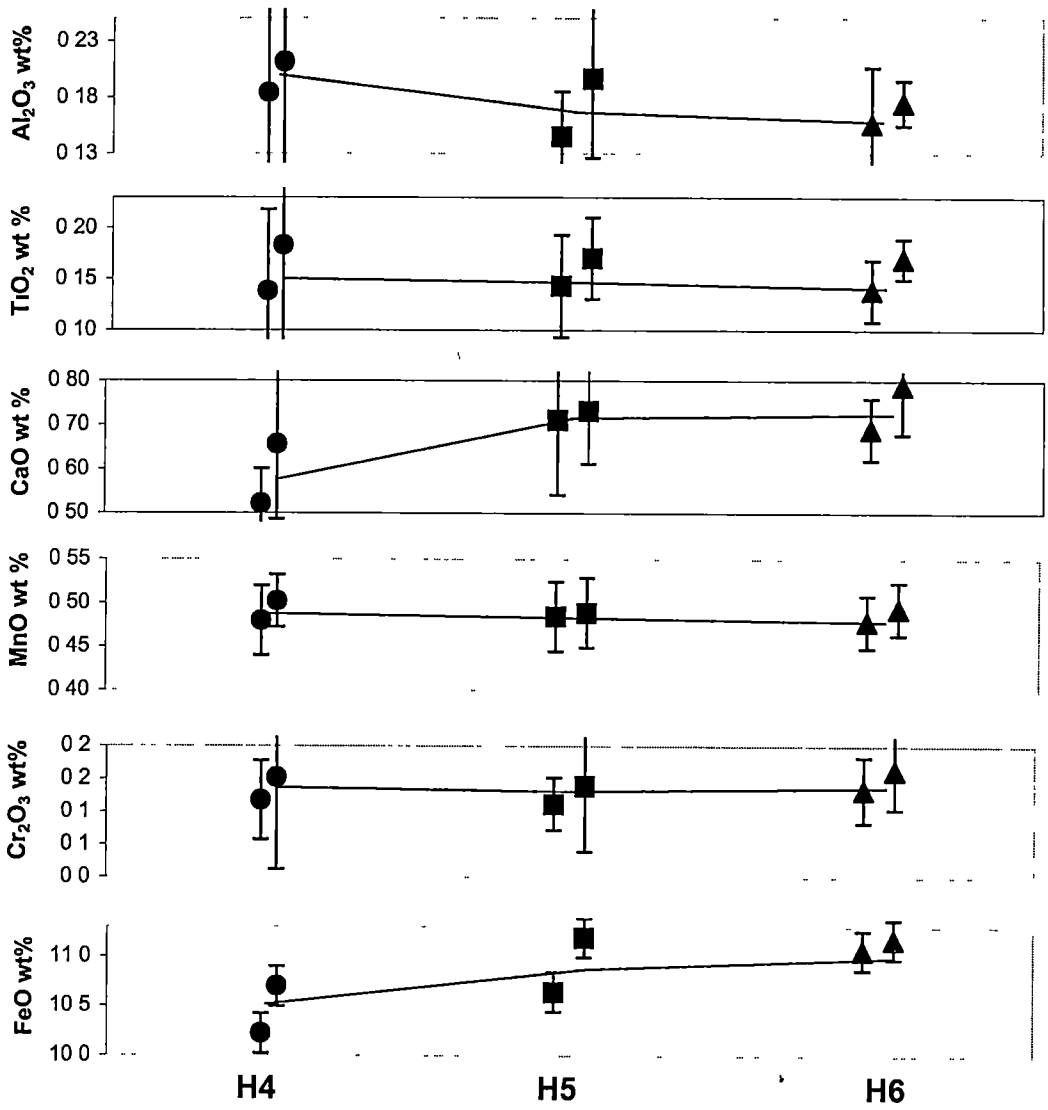

Figure 8: For low-Ca pyroxene minor element abundances, FeO appears to be enriched as metamorphism progresses, but other trends are not as apparent. Error bars show one standard deviation.

FeO is enriched as metamorphism progresses. However, in high-Ca pyroxene there is no apparent pattern for FeO enrichment (fig. 9).

Burnwell

Several graphs showed Burnwell to be distinct from the other chondrites. Comparing olivine/low-Ca pyroxene ratios among the LL4, L4, and H4 chondrites and Burnwell (fig. 10), Burnwell has the lowest value. In fig. 10, the offset between Burnwell and the H group is greater than the offset between H and L, but less than the offset between L and LL. On a diagram showing Fe-Mg-Mn relationships in Burnwell, two H4 chondrites, an L4 chondrite, and an LL4 chondrite (fig. 11), Burnwell olivine and low-Ca pyroxene are depleted in Fe. In addition, Burnwell high-Ca pyroxene is enriched in relation to H4 but depleted in relation to L and LL. However, Burnwell values are far closer to the H4 values than the H4 is to L4 or L4 is to LL4.

In an olivine/low-Ca pyroxene comparison between Burnwell and H4-H6 chondrites (fig. 2), Burnwell plots far below the other meteorites, with error bars not even overlapping the H4 values. When Burnwell olivine and low-Ca pyroxene abundances are analyzed separately against the H4-H6 chondrites (fig. 3), the Burnwell olivine abundance is substantially lower than the other chondrites, well below the H4 values. On the same plot, the low-Ca pyroxene abundance is substantially higher than the other chondrites, although the relation to petrologic trends is clouded by the overlap of the H4, H5, and H6 values.

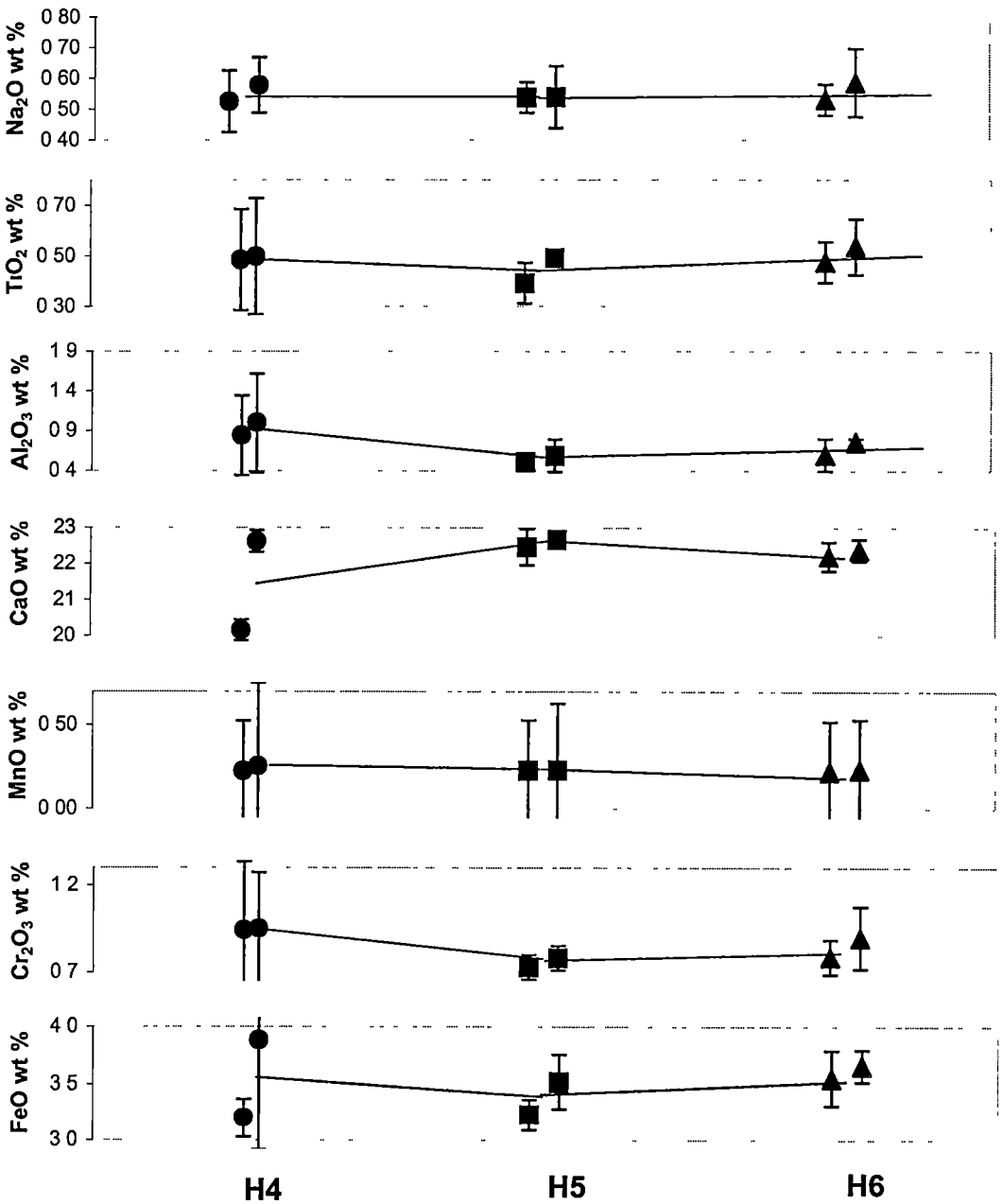

Figure 9: Trends are not apparent in high-Ca pyroxene minor element abundances Error bars show one standard deviation, although some error bars are concealed by data marker.

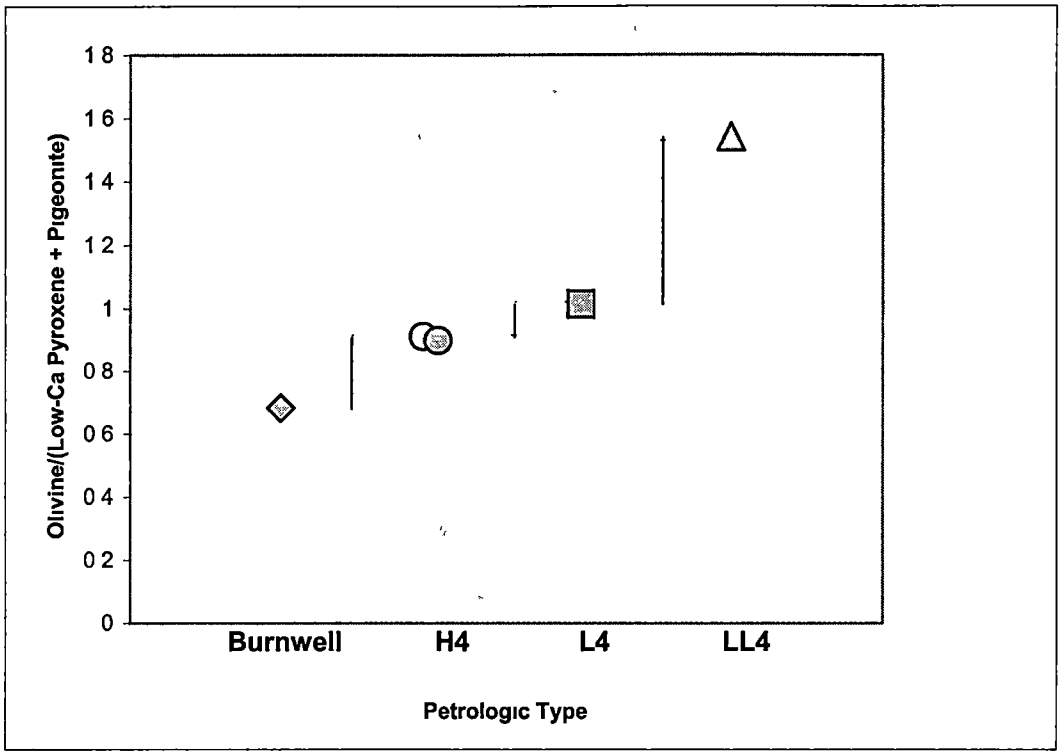

Figure 10: Burnwell lies below olivine/(low-Ca pyroxene + pigeonite) for the meteorites analyzed in Gastineau (2000) and this work. In addition, the gap between the H group and Burnwell is larger than the gap between the L and H groups. The gap may support the classification of Burnwell into its own HH chondritic group.

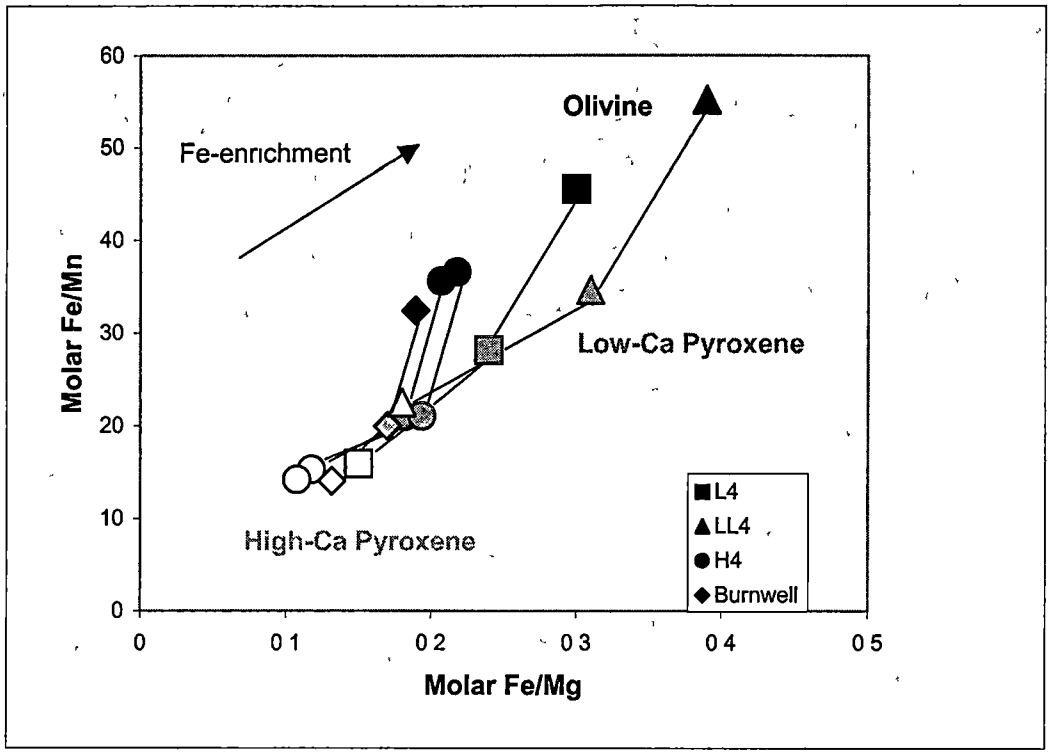

Figure 11: Burnwell lies at the furthest extreme of the H values for olivine and low-Ca pyroxene. However, the distance between the H4, L4, and LL4 values is greater than the distance between Burnwell and H4. Therefore, this diagram does not necessarily support the characterization of Burnwell as its own HH chondritic group. Black symbols are olivine, gray symbols are low-Ca pyroxene, and white symbols are high-Ca pyroxene.

The abundance of plagioclase in Burnwell is also lower than in the other H4 chondrites, again without overlapping error bars (fig. 4). However, the abundance of high-Ca pyroxene in Burnwell is identical to that in the lower of the two H4 chondrites (fig. 5). For Burnwell minor element concentrations in olivine, no clear trends were apparent. However, oxidized Fe was significantly lower than in the other H chondrites — as might be expected from an extremely metal-rich chondrite with strong type 4 character.

For low-Ca pyroxene, only Cr_2O_3 and Al_2O_3 were substantially more abundant than in the other chondrites. However, the concentration of CaO was higher than the other H chondrites, on the opposite side of the trend from the H4 chondrites. FeO concentration was not as depleted as in olivine, but there is a ~0.5 wt% gap between Burnwell values and the lowest H4 values.

In Burnwell high-Ca pyroxene, Burnwell was the most enriched in Na_2O, Al_2O_3, Cr_2O_3, and FeO. However, CaO is substantially depleted for high-Ca pyroxene in relation to the other H chondrites (extending a possible H4 trend).

IV. Discussion

Similarities and differences in normative and modal trends

As Gastineau (2000) found in L and LL chondrites, there is also a discrepancy between normative and modal mineralogies in H chondrites. In graphs relating petrologic type to the ratio of olivine/low-Ca pyroxene (fig. 2), plagioclase concentration (fig. 4), and high-Ca pyroxene concentration (fig. 5), the modes are substantially lower than the norms.

Because the offset is roughly uniform, it may be possible to devise correction factors to apply to the pre-existing sets of ordinary chondrite norms. Gastineau (2000) suggested that the inconsistency, at least for olivine/low-Ca pyroxene, may be due to one or more factors including sample bias in the bulk chemical analysis and/or the thin section, or the inapplicability of the CIPW norm calculation to extremely reduced metal-bearing chondrites. We believe that for at least high-Ca pyroxene and plagioclase, the inconsistency may also result from the presence in the meteorites of a mesostasis that is not considered in the CIPW norm. Additional analyses, including thin sections from various regions of the same meteorite, may help clarify what corrections are needed.

The trend of oxidation with progressive metamorphsim observed in normative minerals by McSween and Labotka (1993) is generally supported by our modal data; however, the similarities are not straightforward. The main reason is that the trends that we observed do not follow a linear progression, and

in many cases, the less metamorphosed H5 chondrites display the most extreme concentrations (or depletions). The overlap of H5 and H6 values is relatively subtle compared with the gap between these chondrites and type 4, and it actually appears to reflect an overlap of H5 and H6 values. From both of our principal oxidation parameters — the ratios of olivine/low-Ca pyroxene and Fe-Mg-Mn relationships — there appears to be some overlap between adjacent petrologic types (including type 4 and type 5). Many of the minor element comparisons also revealed an overlap of H5 and H6 data, but there is a gap between these values and H4 values.

Patterns of overlap may also be present in L and LL data. The olivine/low-Ca pyroxene data in Gastineau (2000) show a type 5-6 overlap with modal LL data and perhaps a type 4-5 overlap with modal type L data. Her plot of normative data also shows the possibility of an overlap of type 4-5 in LL. The normative analyses of McSween and Labotka (1993) showing % fayalite in olivine and % ferrosilite in pyroxene show an H5-H6 overlap in one olivine data set (from Mason, 1974), H4-H5 overlap in another olivine data set (Keil and Fredriksson, 1964), an L5-L6 overlap in both pyroxene data sets (from Mason, 1974; and Keil and Fredriksson, 1964), and an LL4-LL5 overlap in one pyroxene data set (McSween and Patchen, 1989).

The overlap that we observed may suggest that our small data set includes H5 chondrites with olivine, pyroxene, and plagioclase concentrations at the higher end of the H5 range and/or H6 chondrites with properties at the lower end of the

H6 range. The petrographic distinction between type 5 and 6 chondrites is based on broad classifications of near to complete obliteration of primary textures and the extensive development of plagioclase grains (Van Schmus and Wood, 1967). As a consequence, it may be easy to misclassify chondrites that are near the border for classification. Our own observations of these four meteorites indicate that the petrographic distinction between them is not always clear; in fact, one of our H6 meteorites (Chiang Khan) has been classified as both an H5 (Yagi et al., 1989) and an H6 (Clarke, 1982; McSween et al., 1991). A study with a larger data set should clarify whether our observed trends are genuine or whether they are artifacts of sampling size.

Taking into consideration the possibility that petrologic types may overlap, the oxidation trend of McSween and Labotka (1993) was recognized in both our normative and modal data sets. The olivine/low-Ca pyroxene ratio for both norm and mode followed the oxidation trend (fig 2) However, because of differences in H5 normative values, it was impossible to determine if trends were parallel When each mineral was analyzed separately (fig. 3), an increase in olivine abundance was confirmed in both the mode and the norm. Low-Ca pyroxene modal abundance changed little between petrologic types, although the normative trend showed a decrease in abundance with progressive metamorphism — one of the few strong differences between normative and modal mineralogies in our analyses of the H chondrites.

Oxidation with metamorphism is also seen in a comparison of the Fe-Mg-

Mn relationships in olivine, low-Ca pyroxene, and high-Ca pyroxene (fig. 5). The trend was most apparent in olivine, and was least apparent in high-Ca pyroxene. The diffuse data in the diagram may be partially explained by the overlapping nature of chondrite petrologic types as mentioned above.

Normative and modal trends are also roughly parallel in high-Ca pyroxene abundance (fig. 5). Our results agree with Gastineau (2000) in showing an increase with petrologic type, however our relationship between normative and modal mineralogy differs from the relationship expressed in her data. Dodd (1969) observed a strong correlation between petrologic type and the Ca content of pyroxene, with type 4 chondrites containing mostly low-Ca pyroxene and type 5 and 6 containing more calcic pyroxenes. Many of the high-Ca pyroxenes that we observed are very small (less than 10 μm across) and appear to have formed from Ca- and Al-rich mesostasis or along rims of low-Ca pyroxenes, suggesting that Ca diffusion between phases may have also continued.

The main difference between our results and those of Gastineau (2000) is her observation of a convergence between normative and modal high-Ca pyroxene abundances by type 6. We believe that the convergence of high-Ca pyroxene mode and norm abundances in Gastineau's data, in addition to her observation of convergence for plagioclase mode and norm abundances, may result from her exclusion of the SiAl-rich phase from her type 6 analyses.

Both our data and that of Gastineau (2000) show mesostasis in type 6 chondrites (expressed as SiAl-rich phase and K-rich phase in our modal

abundances). The mesostasis has a varied composition, and is enriched in Al and Ca. The CIPW norm does not include a mesostasis in its calculation, and therefore Al-rich and Ca-rich normative phases take up the Al and Ca and appear more abundant. The result is the relatively parallel discrepancy that we observed for H chondrite modal and normative mineralogies (figs. 4 and 5).

However, when Gastineau (2000) did not include the SiAl-rich phase and K-rich phase in her type 6 analyses, the mesostasis ended up in the "unclassified" bin. Because most of the phases in ordinary chondrites are well known and were included in our criteria list, the unclassified category was largely reserved for analyses of cracks or overlapping phases. When Gastineau removed the unclassified elements from her modal analysis totals and normalized the remaining data to 100%, she was also removing the mesostasis phases. This resulted in an artificial inflation of the remaining phases. An artificially enhanced modal value will be more likely to converge with a CIPW normative value, and we believe this is what occurred with the L and LL chondrite plagioclase and high-Ca pyroxene abundances.

Geothermometry in ordinary chondrites

Researchers have applied various geothermometers to ordinary chondrites; however, each method has yielded a different set of temperature values. Using the two-pyroxene geothermometer of Lindsley and Andersen (1983), we calculated peak metamorphic temperatures and compared our results with those

derived by Nakamuta and Motomura (1999) using a sodic plagioclase geothermometer (Table 4). In addition, we show that the Fe-Mg order-disorder closing temperatures in orthopyroxenes observed by Folco et al. (1996) may not affect Fe-Mg-Mn interdiffusion between low-Ca pyroxene, high-Ca pyroxene, and olivine that occurred at higher metamorphic temperatures.

In pyroxene geothermometry, crystallization temperatures are interpreted from the partitioning of Ca between coexisting high-Ca and low-Ca pyroxenes (Lindsley and Andersen, 1983). The pyroxene geothermometer assumes that the two pyroxenes are in equilibrium; however, the high-Ca pyroxene-derived temperature in chondrites, as read from temperature contours on the pyroxene quadrilateral of Lindsley and Andersen (1983), can differ from the low-Ca pyroxene-derived temperature. In their study of LL6 chondrites, McSween and Patchen (1989) determined high-Ca pyroxene temperatures of 900-960°C and low-Ca pyroxene temperatures of 800-900°C. To explain the difference, they suggested that clinoenstatite inverted to the orthopyroxene structure during cooling, and the Ca partitioning between high-Ca pyroxene and clinoenstatite might have been different. They also suggested the possibility that both phases were once in equilibrium, but the low-Ca pyroxene might have re-equilibrated at a lower blocking temperature than the high-Ca pyroxene during cooling. Because high-Ca pyroxene abundance increases during chondrite metamorphsim (Van Schmus and Wood, 1967), McSween and Patchen (1989) favored the high-Ca pyroxene temperatures as representative of peak metamorphism. However, the

Table 4. Geothermometry for H Chondrites

Two-Pyroxene Geothermometery

	Low-Ca Pyroxene[1]	High-Ca Pyroxene[1]	Both Pyroxenes[3]
Canon City (H6)	800°C	675°C	904 ± 45°C
Chiang Khan (H6)	800°C	800°C	877 ± 64°C
Ucera (H5)	800°C	675°C	879 ± 53°C
Allegan (H5)	800°C	625°C	886 ± 43°C
Girgenti (L6)[2]	850°C	790°C	893 ± 47°C
Saint Severin (LL6)[2]	825°C	725°C	895 ± 33°C

Plagioclase Geothermometry[4]

H6	725-742°C
L6	808-820°C
LL6	800°C

1 – Estimated from the graph of Lindsley (1983). Error is ± 50°C.
2 – Pyroxene analyses of Gastineau (2000).
3 – Calculated using the QUILF program of Andersen et al. (1993).
4 – Reported by Nakamuta and Motomura (1999).

pyroxenes may not have reached equilibrium with each other. Many of the high-Ca pyroxene grains occur as rims on low-Ca pyroxene, however we observed a substantial number of grains as an exsolved phase within the Ca-rich mesostasis. In addition, the high-Ca pyroxene appears to not have equilibrated in terms of Fe-Mg-Mn diffusion (fig. 6).

Jones (1997) suggested that the low-Ca pyroxene temperatures may be more accurate, because low-Ca pyroxene appears to equilibrate more rapidly than high-Ca pyroxene during progressive metamorphism. Nakamuta and Motomura (1999) noted that differences in equilibration may be related to the slopes of the pyroxene solvus limbs; for the same temperature interval, a greater change of Ca composition is observed in low-Ca pyroxene than in high-Ca pyroxene. They suggested that the greater high-Ca pyroxene temperatures may be inherited from the original igneous chondrule crystallization, reflecting the sluggish diffusion of Ca at lower temperatures and relatively dry conditions. However, if the two coexisting pyroxenes never equilibrated, then thermodynamically the pyroxene geothermometer may not be appropriate for our chondrites.

Our data show Fe-enrichment in olivine and low-Ca pyroxene with increased metamorphism but a diffuse trend in high-Ca pyroxene (fig. 6). The patterns suggest that Fe-Mg-Mn diffusion in olivine is fastest, slower in low-Ca pyroxene, and slowest in high-Ca pyroxene. Ca diffusion is slower than Fe, Mg, and Mn (Jurewicz and Watson, 1988), so Figure 6 suggests that high-Ca pyroxene may not have reached equilibrium. Either Jones (1997) is correct that high-Ca

pyroxenes reflect pre-accretionary igneous crystallization temperatures, or the olivines and low-Ca pyroxenes have re-equilibrated at lower temperatures. From Figure 6 and an analysis of high-Ca pyroxene minor element data, it appears that the first suggestion may be correct and high-Ca pyroxene yields only pre-accretionary temperatures.

Because of the possibility that our H5 and H6 chondrites experienced similar metamorphism, we graphically determined temperatures for all four of these meteorites using the Lindsley (1983) geothermometer (Table 4). We also determined temperatures for L6 and LL6 chondrites using the pyroxene analyses of Gastineau (2000). Given the uncertainties, these temperatures are similar and it may be possible to assume equilibrium. Therefore, we also report calculated two-pyroxene temperatures using the QUILF program of Andersen et al. (1993), which takes minor elements in pyroxenes into account (Table 4). While our type 5 and type 6 chondrites had overlapping temperatures, Allegan (H5) had the lowest high-Ca pyroxene temperature of 600-650°C and Chiang Khan had the highest with 800°C. Low-Ca pyroxene temperatures were similar among all four H chondrites, although the average (~800°C) was much greater than the average of the greatest high-Ca pyroxene temperatures (~740°C). From the one L6 chondrite of Gastineau (2000), we derived temperatures of 850°C for low-Ca pyroxene and 775-800°C for high-Ca pyroxene. From one LL6 chondrite of Gastineau (2000) we derived temperatures of 800-850°C for low-Ca pyroxene and 675-775°C for high-Ca pyroxene. Our results do not follow the trend for

pyroxene-derived temperatures in LL chondrites by McSween and Patchen (1989), who found higher temperatures for high-Ca pyroxenes, but they may support studies that suggest that L and LL chondrites were subjected to higher temperatures than H chondrites (e.g., Nakamuta and Motomura, 1999; Olsen and Bunch, 1984). A larger data set will be necessary to determine whether our values are valid and why our values and trends differ from those of McSween and Patchen (1989).

The plagioclase geothermometer (e.g., Nakamuta and Motomura, 1999) is based on disordering of Si and Al in the crystal lattice of sodic plagioclase with increasing temperature. Nakamuta and Motomura (1999) analyzed several sections from three H6 chondrites, two L6 chondrites, and one LL6 chondrite, and found temperature ranges of 725-742°C for H6, 808-820°C for L6, and 800°C for LL6. The spread of our pyroxene temperature values makes a direct comparison difficult, but the plagioclase values are generally within our range of data.

The plagioclase thermometer relies upon thermodynamic influences within a single crystal, and therefore does not depend on the diffusion of ions between two minerals. A range of ordering is observed within plagioclase grains in a given chondrite, and Nakamuta and Motomura (1999) selected the least ordered plagioclase grains that they could identify. However, even the least ordered grains may not represent the peak metamorphic conditions if no new plagioclase was forming under type 6 conditions.

While mesostasis is observed in our H6 chondrites, plagioclase abundance

does not appear to increase after type 5 (fig. 4). Our analyses agree with earlier studies (e.g., Sears et al., 1980) that suggest plagioclase has largely crystallized by type 5 conditions. If this is true, then temperatures recorded by the plagioclase thermometer would be type 5 temperatures, not the peak chondrite temperatures of type 6. However, to determine peak metamorphic temperatures the most equilibrated type 6 chondrites need to be analyzed.

Folco et al. (1996) measured ordering of Fe and Mg in orthopyroxene within unshocked H chondrites and arrived at closure temperatures of approximately 380-480°C for all three petrologic types, reflecting post-metamorphic cooling. They suggest that the various chondrite petrologic types all experienced similar temperature-time conditions when they cooled through this interval. Our analyses show that even if ordering reflects a period of cooling, Fe-Mg-Mn interdiffusion between pyroxenes and olivine within H chondrites changes progressively with metamorphism and is retained in these phases (fig. 6). A similar progression can also be seen in the average Fe-Mg ratios for orthopyroxenes in H4 (0.196), H5 (0 197), and H6 (0.208) chondrites from the data of Folco et al. (1996), as well as for pyroxenes and olivine in L and LL chondrites (Gastineau, 2000).

Applications to the search for the H6 parent body

Gaffey and Gilbert (1998) used the normative mineral abundances of McSween and Labotka (1993) — ultimately derived from McSween et al. (1991)

— to calculate average H chondrite spectra and link these spectra to 6 Hebe. In addition, Gaffey and Gilbert (1998) used the same data set to determine the effects of impacts on the FeNi metal abundances at the surface of 6 Hebe (although many researchers attribute the observed spectral reddening to space weathering, not metal). Because our study suggests that normative and modal data are not identical, spectral comparisons are drawn into question. However, because Gaffey and Gilbert used averaged values, the overlap between 6 Hebe spectra and H chondrite spectra will probably persist, even if the specific values of their data set change.

Gaffey and Gilbert (1998) also used the Fe oxidation mechanism of McSween and Labotka (1993) to link 6 Hebe more generally to the H chondrites. Because the link is based upon a normative mineral trend that is also paralleled in the modal minerals, the comparison should be unaffected. However, with similarities in H5 and H6 chondrites adding confusion to the oxidation trend, care should be taken in how the trend is applied to spectral variation (Gaffey and Gilbert 1998). Because none of our results appear to invalidate the data presented by Gaffey and Gilbert (1998) and others, we believe 6 Hebe remains the leading candidate for the H chondrite parent body.

Burnwell's place among the ordinary chondrites

In almost every analysis, the low-FeO, type 4 chondrite Burnwell remains unique, although like Russell et al. (1998), we found Burnwell to be most similar

to the H4 chondrites. In plots comparing Burnwell to the H4-H6 chondrites, Burnwell abundances lie on the H4 side of the graphs, often appearing to be an extreme extension of these values (figs. 2-4). In addition, the modes we determined for Burnwell show the same discrepancy between norm and mode as is seen in the H chondrites (fig. 12).

The graphs of olivine/low-Ca pyroxene (figs. 2 and 10) are the most suggestive of Burnwell representing a new group — although they are not wholly convincing In these graphs, Burnwell plots far below the other chondrites, farther from the H4 chondrites than the H4 chondrites are from the L4 chondrites. When olivine and low-Ca pyroxene are analyzed separately (fig. 3). In addition, Burnwell low-Ca pyroxene abundance is substantially higher than in the other chondrites, while olivine abundance is substantially lower than in the other chondrites. The abundance of plagioclase in Burnwell is also substantially lower than in the other type 4 chondrites (fig. 4), and Burnwell contains the highest abundance of the SiAl-rich component (Table 3), suggesting abnormally high concentrations of glass However, the concentration of high-Ca pyroxene in Burnwell is identical to the concentration in the lower of the two H4 chondrites (Farmville), again implying greater similarities to the H4 chondrites.

On the Fe-Mg-Mn plot (fig. 11), Burnwell olivine and low-Ca pyroxene phases are depleted in Fe, while the high-Ca pyroxene phase is enriched, relative to the other chondrites (including H4). This would seem to suggest that Burnwell is independent of the H group; however, for both olivine and low-Ca pyroxene,

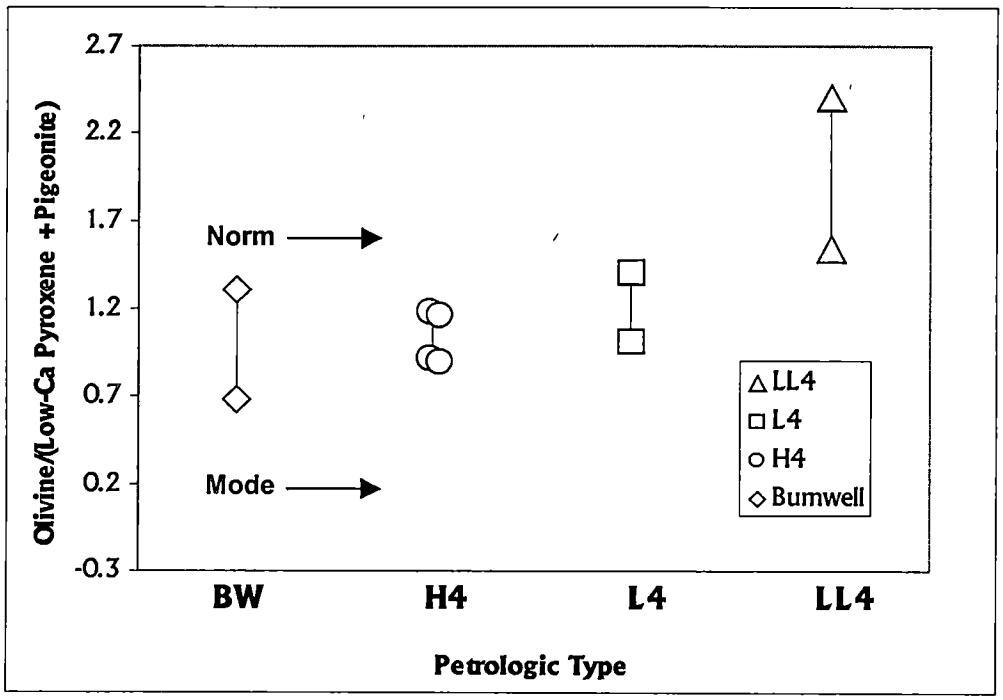

Figure 12: Type 4 ordinary chondrites in this study and those analyzed by Gastineau (2000) display a discrepancy between mineral abundances determined with the CIPW normative mineralogy calculation and modal mineral abundances. The diagram above demonstrates the discrepancy for the ratio of olivine/(low-Ca pyroxene + pigeonite) and references our data for Burnwell and H4, and the data of Gastineau (2000) for L4 and LL4 data.

Burnwell plots much closer to H4 chondrites than H4 plots in relation to L4, or L4 plots in relation to LL4. The minor element concentrations for Burnwell followed similar patterns, although the most obvious was the FeO depletion in olivine and low-Ca pyroxene and enrichment in high-Ca pyroxene. Generally, the low-Ca pyroxene Cr_2O_3 was substantially more abundant, as was olivine Al_2O_3 and CaO The CaO abundance is opposite the trend of the H4 chondrites, which may reflect the overall lack of high-Ca pyroxene in Burnwell. In high-Ca pyroxene, CaO is actually depleted far below the other chondrites and FeO is more abundant, although the overlap of the data makes any H4-H6 trend impossible to distinguish. Burnwell high-Ca pyroxene was also the most enriched in Na_2O, Al_2O_3, and Cr_2O_3

Because Burnwell plotted as the farthest extreme for type 4 chondrites on most, but not all, graphs and because those extremes were generally large, it may well represent a distinct type of chondrite. However, without any type 5 or type 6 low-FeO chondrites to compare to Burnwell, our studies do not resolve whether Burnwell actually represents a new high bulk Fe, "HH" group

V. Conclusions

Our research concludes that the mineral abundances computed for H chondrites by the CIPW normative calculation are significantly different from the modal abundances determined for these meteorites. The discrepancy may result in part from the failure of the CIPW calculation to account for the Al- and Ca-enriched mesostasis phase that is found in ordinary chondrites of all petrologic types

The discrepancy is relatively uniform from chondrite to chondrite and does not greatly affect mineralogic trends with metamorphism that were identified using normative calculations (McSween and Labotka, 1993). We determined the variations in the modal ratio of olivine/low-Ca pyroxene in H chondrites and found that olivine does increase in abundance, supporting the oxidation trend. We also plotted modal Fe-Mg-Mn relationships and found that oxidized Fe abundances within olivine and pyroxenes increase with petrologic type, relative to Mg and Mn.

Over the course of the study, it also became apparent that data from adjacent petrologic types frequently overlapped, particularly for H5 and H6 chondrites. The overlap may be an artifact of our small data set or the misclassification of one or more of our equilibrated chondrites. However, overlap also appears in L and LL chondrite data (e.g., Gastineau, 2000; McSween and Labotka, 1993) and may actually be the result of the gradational nature of ordinary chondrite metamorphism. Petrologic trends may be more apparent from

analyses of a wider range of petrologic types, as opposed to observations of adjacent petrologic types.

We conclude that plagioclase crystallized completely by type 5, otherwise type 6 abundances would be substantially higher than type 5 abundances. While Al- and Si-rich mesostasis remains in type 6 chondrites, the plagioclase component appears to have devitrified completely during petrologic type 5 metamorphism. Therefore, thermometers which rely on plagioclase crystallizing during type 6 metamorphism may not be valid. However, the alternative — the two-pyroxene geothermometer — has its own pitfalls when applied to ordinary chondrites. If the pyroxene geothermometry for our specimens is valid, our data may suggest a greater agreement between low-Ca and high-Ca pyroxene temperatures than previously found and closer agreement with plagioclase geothermometry than earlier comparisons.

We also provide additional data confirming that Burnwell is unique among the known ordinary chondrites, although its differences may not be sufficient to confirm a new HH group. Hopefully, additional low-FeO falls will find their way into research collections, and the classification can be determined in the light of petrologic types other than type 4.

Because normative and modal data are not identical, the previous applications of normative data to asteroid spectroscopy should be revisited. While trends and overall conclusions probably will not need adjustment, the comparisons between asteroid and H chondrite spectra may need to be re-

evaluated. Since overall conclusions should persist in the light of new modal data, we still believe that asteroid 6 Hebe represents the best candidate for an H chondrite parent body.

Bibliography

Bibliography

Andersen D. J., Lindsley D. H., and Davidson P. M. (1993) QUILF. A Pascal program to assess equilibria among Fe-Mg-Mn-Ti oxides, pyroxenes, olivine, and quartz. *Computers Geosci.* **19**, 1333-1350.

Bennett M. E. III and McSween H. Y., Jr. (1996) Revised model calculations for the thermal histories of ordinary chondrite parent bodies. *Meteor. Planet. Sci.* **31**, 783-792.

Brett R. and Sato M. (1984) Intrinsic oxygen fugacity measurements on seven chondrites, a pallasite, and a tektite and the redox state of meteorite parent bodies. *Geochim Cosmochim Acta* **48**, 111-120.

Bryan W. B. and Kullerud G. (1975) Mineralogy and chemistry of the Ashmore chondrite. *Meteoritics* **10**, 41-51.

Bunch T. E., Mall A. P., and Lewis C. F. (1972) The Seoni chondrite. *Meteoritics* **7**, 87-95.

Clarke R. S. Jr. (1982) Fall of the Chiang Khan, Thailand, stony meteorite. *Meteoritics* **17**, 93-97.

Cloutis E. A., Gaffey M. J., Jackowski T. L. and Reed K. L. (1986) Calibrations of phase abundance, composition, and particle size distribution for olivine-orthopyroxene mixtures from reflectance spectra. *J.Geophys. Res.* **91**, 11641-11,653.

Dodd R T. (1969) Metamorphism of the ordinary chondrites: A review. *Geochim Cosmochim Acta* **33**, 161-203.

Folco L., Mellini M. and Pillinger, C. T. (1996) Unshocked equilibrated H-chondrites: A common low-temperature record from orthopyroxene iron-magnesium ordering. *Meteoritics* **31**, 388-393.

Fudali R. F. and Noonan A. F. (1975) Gobabeb, a new chondrite: The coexistence of equilibrated silicates and unequilibrated spinels. *Meteoritics* **10**, 31-39.

Gaffey M. J. and Gilbert S. L. (1998) Asteroid 6 Hebe: The probable parent body of the H-type ordinary chondrites and the IIE Fe meteorites. *Meteor. Planet. Sci.* **33**, 1281-1295.

Gastineau H. (2000) A test for oxidation during metamorphism of L and LL chondrites. A thesis presented for the Master of Science Degree at The University

of Tennessee.

Ghosh A. and McSween H. Y. Jr. (2000) The effect of incremental accretion on the thermal modeling of asteroid 6 Hebe. *Meteor. Planet. Sci.* **35**, A59.

Goodrich C. A. and Delaney J. S. (2000) Fe/Mg-Fe/Mn relations of meteorites and primary heterogeneity of primitive achondrite parent bodies. *Geochim. Cosmochim Acta* **64**, 149-160.

Gomes C. B. Keil K. and Jarosewich E. (1977) Studies of Brazillian Meteorites VIII. Mineralogy, petrology and chemistry of the Itapicuru Mirim, Maranhão, chondrite. *An. Acad. Brasil Ciênc.* 49, 407-412.

Gopel C., Manhès G. and Allègre C. J. (1994) U-Pb systematics of phosphates from equilibrated ordinary chondrites. *Earth Planet. Sci. Lett* **121**, 153-171.

Grady M. M. (2000) Catalogue of meteorites Cambr. Univ. Press, 5th ed.

Jaques A. L., Lowenstein P. L., Green D. H., Kiss E., Nance W. B., Taylor S. R. and Ware N. G. (1975) The Ijopega chondrite: A new H6 fall. *Meteoritics* **10**, 289-301.

Jones R. H. (1997) Petrology and mineralogy of type II, FeO-rich, chondrules in Semarkona (LL3.0): Origin by closed-system fractional crystallization, with evidence for supercooling. *Geochim. Cosmochim. Acta* **54**, 1785-1802.

Jurewicz A. J. G. and Watson E. B. (1988) Cations in olivine, Part 2: Diffusion in olivine xenocrysts with applications to petrology and mineral physics. *Contrib. Mineral Petrol.* **99**, 186-201.

Keil K. and Fredriksson K. (1964) The Fe, Mg, and Ca distribution in coexisting olivines and rhombic pyroxenes of chondrites. *J. of Geophys. Res.* **69**, 3487-3515

Krot A., Ivanova M. A., and Wasson J. T.. (1993) The origin of chromitic chondrules and the volatility of Cr under a range of nebular conditions. *Earth Planet Sci Lett.* **119**, 569-584.

Lange D. E , Frost K., Sipiera P. P., and Moore C. B. (1974) The Canyonlands meteorite. *Meteoritics* **9**, 271-280.

Lindsley D. H. (1983) Pyroxene geothermometry. *Amer Mineral.* **68**, 477-493.

Lindsley D. H. and Andersen D. J. (1983) A two-pyroxene thermometer. *J. of Geophys. Res.* **88**, A887-A906.

McSween H. Y. Jr., Bennett M. E. III, and Jarosewich E. (1991) The mineralogy of ordinary chondrites and implications for asteroid spectrophotometry. *Icarus* **90**, 107-116.

McSween H. Y. Jr. and Labotka T. C. (1993) Oxidation during metamorphism of the ordinary chondrites. *Geochim. Cosmochim Acta* **57**, 1105-1114.

McSween H. Y. Jr and Patchen A. D. (1989) Pyroxene thermobarometry in LL-group chondrites and implications for parent body metamorphism. *Meteoritics* **24**, 219-226.

Nakamuta, Y. and Motomura, Y. (1999) Sodic plagioclase thermometry of type 6 ordinary chondrites; implications for the thermal histories of parent bodies. *Meteor Planet Sci* **34**, 763-772.

Miyamoto M., Fujii N., and Takeda H. (1981) Ordinary chondrite parent body: An internal heating model. *Proc of the Lunar Planet Sci Conf. 12B*, 1145-1152.

Olsen E. J., Bunch T. E. (1984) Equilibration temperatures of the ordinary chondrites: a new evaluation. *Geochim. Cosmochim Acta* **48**, 1363-1365.

Russell S. S., McCoy T. J., Jarosewich E. and Ash R. D. (1998) The Burnwell, Kentucky, low Fe oxide chondrite fall: Description, classification, and origin. *Meteor. Planet. Sci.* **33**, 853-856.

Scott E. R. D. and Rajan R. S. (1981) Metallic minerals, thermal histories and parent bodies of some xenolithic, ordinary chondrite meteorites. *Geochim et Cosmochim Acta* **45**, 53-67.

Sears D.W., Grossman J. N., Melcher C. L., Ross L. M., Mills A. A. (1980) Measuring metamorphic history of unequilibrated ordinary chondrites. *Nature* **287**, 791-795.

Sears D. W. G. and Weeks K. S. (1986) Chemical and physical studies of type 3 chondrites — VI: Siderophile elements in ordinary chondrites. *Geochim et Cosmochim Acta* **50**, 2815-2832.

Taylor G. J., Maggiore P., Scott E. R. D., Rubin A. E. and Keil K. (1987) Original structures, and fragmentation and reassembling histories of asteroids: Evidence from meteorites. *Icarus* **69**, 1-13.

Taylor L.A., Patchen A., Taylor D.H. S. and Chambers J. G. (1996) X-Ray digital imaging petrography of lunar mare soils: modal analyses of minerals and glasses. *Icarus* **124**, 500-512.

Urey H.C. and Craig H. (1953) The composition of the stone meteorites and the origin of the meteorites. *Geochim et Cosmochim Acta* **4**, 36-82.

Van Schmus W. R. and Wood J, A. (1967) A chemical-petrologic classification for the chondritic meteorites. *Geochim et Cosmochim Acta* **31**, 747-765.

Wang D. and Rubin A. E. (1987) Petrology of nine ordinary chondrite falls from China. *Meteoritics* **22**, 97-104.

Williams J.G. (1973) Meteorites from the asteroid belt. *EOS* (Trans. Amer. Geophys. Union) **54**, 233.

Williams J. G. and Faulkner J. (1981) The position of secular resonance surfaces. *Icarus* **46**, 390-399.

Wisdom J. (1985) A perturbative treatment of motion near the 3/1 commensurability. *Icarus* **63**, 272-289.

Yagi K., Kimura M., Kuroda Y. and Momose K. (1989) Petrology and magnetic properties of the Chiang Khan, Thailand, meteorite. *Mineral Petrol.* **40** 173-182.

Appendices

Appendix 1A: Canon City (H6)

	Area %	Area % w/o unclassified	Density of Phase	Mode	Mode (in %)	Normative Mineralogy	{McSween et al , 1991}
sial	2 76	2 93	2 66	7 79	2 04		sial
kphase	0 29	0 31	2 54	0 78	0 21	0 47	orthoclase
phosphate	0 62	0 66	3 10	2 04	0 54	0 71	apatite
ilmenite	0 01	0 01	4 78	0 05	0 01	0 26	ilmenite
chromite	0 65	0 69	5 06	3 49	0 92	0 79	chromite
kamacite	7 42	7 87	7 90	62 2	16 3	18 8	metal (kam + tae)
taenite	0 59	0 63	8 14	5 09	1 34		
FeS	4 30	4 56	4 84	22 1	5 79	5 61	FeS
pig	1 36	1 44	3 44	4 96	1 30		
cpx	3 49	3 70	3 28	12 1	3 19	4 53	diopside
plagioclase	8 41	8 92	2 62	23 4	6 13	9 21	anorthite + albite
opx	32.4	34 4	3 42	118	30 9	25 4	hypersthene (opx+pig)
oliv	32 0	33 9	3 52	119	31 3	34 1	oliv
unclassified	5 70						
Total	100 0	100 0		380 9	100 0	100 0	
Total - unclassified	94 3						
				ol/opx	1 014		
				ol/(opx+pig)	0 973		

Appendix 1B: Chiang Khan (H6)

	Area %	Area % w/o unclassified	Density of Phase	Mode	Mode (in %)	Normative Mineralogy	{McSween et al , 1991}
sial	3 99	4 27	2 66	11 4	3 02		sial
kphase	0 31	0 33	2 54	0 84	0 22	0 48	orthoclase
phosphate	0 63	0 67	3 10	2 09	0 56	0 57	apatite
ilmenite	0 02	0 02	4 78	0 10	0 03	0 25	ilmenite
chromite	0 73	0 78	5 06	3 95	1 05	0 74	chromite
kamacite	6 44	6 89	7 90	54 4	14 5	18 0	metal (kam + tae)
taenite	0 49	0 52	8 14	4.27	1.13		
FeS	4.74	5 07	4 84	24 5	6 52	5 22	FeS
pig	1 81	1 94	3 44	6 66	1 77		
cpx	3 27	3 50	3 28	11 5	3 05	4 07	diopside
plagioclase	7 77	8 31	2 62	21 8	5.79	9 71	anorthite + albite
opx	31 0	33 1	3 42	113	30 1	26 4	hypersthene (opx+pig)
oliv	32 4	34 6	3 51	121	32 3	34 6	oliv
unclassified	6 49						
Total	100 0	100 0		376 1	100 0	100 0	
Total - unclassified	93 5						
				ol/opx.	1 073		
				ol/(opx+pig)	1 013		

Appendix 1C: Ucera (H5)

	Area %	Area % w/o unclassified	Density of Phase	Mode	Mode (in %)	Normative Mineralogy	{McSween et al , 1991}
sial	3 46	3 66	2 66	9 73	2 58		sial
kphase	0 56	0 59	2 54	1 50	0 40	0 53	orthoclase
phosphate	0 54	0 57	3 10	1 77	0 47	0 62	apatite
ilmenite	0 02	0 02	4 78	0 10	0 03	0 21	ilmenite
chromite	0 88	0 93	5 06	4 71	1 25	0 77	chromite
kamacite	6 16	6 52	7 90	51.5	13 6	16 5	metal (kam + tae)
taenite	0 83	0 88	8 14	7 15	1 89		
FeS	5 70	6 03	4 84	29 2	7 73	6 00	FeS
pig	1 94	2 05	3 44	7 06	1 87		
cpx	3 54	3 74	3 28	12 3	3 25	4 34	diopside
plagioclase	7 88	8 33	2 62	21 8	5 78	8 99	anorthite + albite
opx	30 6	32 4	3 41	110	29 2	26 4	hypersthene (opx+pig)
oliv	32 4	34 3	3 51	120	31 9	35 6	oliv
unclassified	5 44						
Total	100 0	100 0		377 6	100 0	100 0	
Total - unclassified	94 6						
				ol/opx	1 091		
				ol/(opx+pig)	1 025		

Appendix 1D: Allegan (H5)

	Area %	Area % w/o unclassified	Density of Phase	Mode	Mode (in %)	Normative Mineralogy	{McSween et al , 1991}
sial	3 92	4 32	2 66	11 5	3 09		sial
kphase	0 35	0 39	2 54	0 98	0 26	0 53	orthoclase
phosphate	0 52	0 57	3 10	1 78	0 48	0 64	apatite
ilmenite	0 04	0 04	4 78	0 21	0 06	0 19	ilmenite
chrome	0 75	0 83	5 06	4 19	1 12	0 80	chromite
kamacite	5 60	6 18	7 90	48 8	13 1	19 8	metal (kam + tae)
taenite	0 51	0 56	8 14	4 58	1 23		
FeS	4 95	5 46	4 84	26 4	7 09	5 54	FeS
pig	1 80	1 99	3 44	6 83	1 83		
cpx	3 25	3 59	3 28	11 8	3 15	4 14	diopside
plagioclase	7 78	8 58	2 62	22 5	6 03	8 44	anorthite + albite
opx	29 6	32 7	3.41	111	29 9	29 0	hypersthene (opx+pig)
oliv	31 6	34 8	3 50	122	32 7	30 9	oliv
unclassified	9 35						
Total	100 0	100 0		372 8	100 0	100 0	
Total - unclassified	90 6						
				ol/opx	1 093		
				ol/(opx+pig)	1 030		

Appendix 1E: Farmville (H4)

	Area %	Area % w/o unclassified	Density of Phase	Mode	Mode (in %)	Normative Mineralogy	{McSween et al , 1991}
sial	5 76	6 28	2 66	16 7	4 40		sial
kphase	0 63	0 69	2 54	1 74	0 46	0 54	orthoclase
phosphate	0 54	0 59	3 10	1 82	0 48	0 62	apatite
ilmenite	0 01	0 01	4 78	0 05	0 01	0 21	ilmenite
chrome	0 70	0 76	5 06	3 86	1 02	0 73	chromite
kamacite	6 82	7 43	7 90	58 7	15 5	18 5	metal (kam + tae)
taenite	0 59	0 64	8 14	5 23	1 38		
FeS	5 47	5 96	4 84	28 8	7 61	5 00	FeS
pig	3 46	3 77	3 44	13 0	3 42		
cpx	2 09	2 28	3 28	7 47	1 97	3 83	diopside
plagioclase	5 37	5 85	2 62	15 3	4 04	8 72	anorthite + albite
opx	30 6	33 3	3 40	113	29 9	28 6	hypersthene (opx+pig)
oliv	29 8	32 4	3 49	113	29 8	33 3	oliv.
unclassified	8 20						
Total	100 0	100 0		379 2	100 0		
Total - unclassified	91 8						
				ol/opx	0 999		
				ol/(opx+pig)	0 896		

Appendix 1F: Avanhandava (H4)

	Area %	Area % w/o unclassified	Density of Phase	Mode	Mode (in %)	Normative Mineralogy	{McSween et al , 1991}
sial	5 15	5 68	2 66	15 1	3 98		sial
kphase	0 36	0 40	2 54	1 01	0 27	0 53	orthoclase
phosphate	0 57	0 63	3 10	1 95	0 51	0 62	apatite
ilmenite	0 00	0 00	4 78	0 00	0 00	0 23	ilmenite
chrome	0 62	0 68	5 06	3 46	0 91	0 71	chromite
kamacite	6 74	7 43	7 90	58 7	15 5	18 2	metal (kam + tae)
taenite	0 55	0 61	8 14	4 93	1 30		
FeS	5 31	5 85	4 84	28 3	7 47	5 48	FeS
pig	2 07	2 28	3 44	7 85	2 07		
cpx	2 81	3 10	3 28	10 2	2 68	3 76	diopside
plagioclase	6 11	6 74	2 62	17 6	4 65	8 65	anorthite + albite
opx	31 1	34 2	3 41	117	30 8	28 4	hypersthene (opx+pig)
oliv	29 4	32 4	3 50	113	29 9	33 4	oliv
unclassified	9.29						
Total	100 0	100 0		379 2	100 0		
Total - unclassified	90 7						
				ol/opx	0 971		
				ol/(opx+pig)	0 910		

Appendix 1G: Burnwell

	Area %	Area % w/o unclassified	Density of Phase	Mode	Mode (in %)	Normative Mineralogy	{McSween et al , 1991}
sial	6 70	7 29	2 66	19 4	5 12	n/a	sial
kphase	0 49	0 53	2 54	1 35	0 36	0 54	orthoclase
phosphate	0 51	0 55	3 10	1 72	0 45	0 64	apatite
ilmenite	0 00	0 00	4 78	0 00	0 00	0 19	ilmenite
chrome	0 60	0 65	5 06	3 30	0 87	0 81	chromite
kamacite	7 08	7 70	7 90	60 8	16 1	19 7	metal (kam + tae)
taenite	0 44	0 48	8 14	3 89	1 03	n/a	
FeS	5 20	5 65	4 84	27 4	7 23	3 64	FeS
pig	5 83	6 34	3 44	21 8	5 76	n/a	
cpx	2 09	2 27	3 28	7 45	1 97	3 39	diopside
plagioclase	3 77	4 10	2 62	10.7	2 84	8 97	anorthite + albite
opx	33 1	36 0	3 40	122	32 3	26 9	hypersthene (opx+pig)
oliv	26 1	28 4	3 46	98 2	25 9	35 2	oliv
unclassified	8 05					0 08	cobalt
Total	100 0	99 9		378 4	100 0	100 0	
Total - unclassified	91 91						
			ol/opx	0 802			
			ol/(opx+pig)	0 681			

Appendix 2: Olivines (wt%)

	H6 Canon City [18]	H6 Chiang Khan [18]	H5 Ucera [24]	H5 Allegan [24]	H4 Farmville [48]	H4 Avanhandava [45]	HH4 Burnwell [34]
SiO2	38 8 (2)	39 2 (2)	39.2 (2)	39 2 (4)	39 7 (3)	39.2 (5)	39.5 (3)
Al2O3	<0 03	<0 03	<0.03	<0 03	<0.03	<0.03	<0.03
MgO	42 6 (5)	42.6 (3)	43 2 (3)	43.5 (4)	43.7 (3)	43 2 (3)	45 1 (6)
Na2O	<0.03	<0 03	<0.03	<0 03	<0.03	<0.03	<0 03
CaO	<0 03	<0.03	<0 03	0 03 (1)	0 04 (3)	0.04 (6)	<0.03
TiO2	<0.03	<0 03	<0.03	<0 03	<0.03	<0.03	0.04 (5)
FeO	18.1(6)	17.6 (2)	17 6 (3)	16 8 (6)	16.2 (3)	16 8 (2)	15.2 (5)
MnO	0 45(3)	0 46 (3)	0 45 (4)	0.46 (4)	0 45 (3)	0.46 (3)	0 47 (3)
Cr2O3	0 03(3)	0.03 (3)	0 03 (3)	<0.03	<0 03	<0.03	0 04 (3)
Total	100 0	99 9	100 4	100 0	100 2	99.6	100.4
Cations based on 4 oxygens							
Si	0 990	0 998	0 993	0.994	1 001	0 996	0 991
Al	0 000	0.000	0 000	0 000	0 000	0 000	0 000
Mg	1 622	1 616	1 631	1 644	1.644	1 637	1 684
Na	0 000	0.000	0.000	0 000	0.000	0 000	0 001
Ca	0 001	0 001	0 001	0 001	0 001	0 001	0 001
Ti	0 000	0 000	0.000	0 000	0.000	0 000	0 001
Fe	0.386	0.376	0 372	0 356	0.340	0 357	0.319
Mn	0 010	0.010	0 010	0.010	0 010	0 010	0 010
Cr	0 001	0.001	0 001	0 000	0 000	0 000	0 001
Total	3 009	3 001	3 007	3 005	2 998	3 002	3 007
Fe/Mn	40 43	37 36	38.50	36 05	35.52	36 51	32 38
Fe/Mg	0 238	0.233	0.228	0 216	0 207	0 218	0 189

1 -- For all tables, ratios may appear incorrect because they are based upon averaged values that were not rounded

2 -- For all tables, number of analyses appears in brackets

Appendix 3: Low-Ca Pyroxenes (wt%)

	H6 Canon City [20]	H6 Chiang Khan [22]	H5 Ucera [21]	H5 Allegan [22]	H4 Farmville [44]	H4 Avanhandava [45]	HH4 Burnwell [43]
SiO2	55 8 (3)	56.2 (4)	56.1 (4)	56.4 (5)	57.1 (3)	56.6 (4)	56 3 (8)
Al2O3	0.18 (2)	0 16 (5)	0.15 (4)	0 20 (7)	0 18 (15)	0 21 (17)	0 53 (57)
MgO	31 0 (1)	30.7 (3)	31.3 (3)	31.5 (1)	31.5 (2)	31 0 (3)	31.9 (11)
Na2O	<0.03	<0 03	<0.03	<0.03	<0 03	<0 03	0 05 (7)
CaO	0.79 (11)	0.69 (7)	0.73 (12)	0 71 (17)	0 52 (8)	0 66 (17)	0.87 (105)
TiO2	0 17 (2)	0.14 (3)	0.14 (5)	0.17 (4)	0 14 (8)	0 18 (10)	0.15 (9)
FeO	11 2 (2)	11 1 (2)	11.2 (2)	10.6 (2)	10.2 (2)	10 7 (2)	9.66 (49)
MnO	0.48 (3)	0 49 (3)	0.49 (4)	0.49 (4)	0.48 (4)	0 50 (3)	0 48 (5)
Cr2O3	0.16 (6)	0 13 (5)	0.11 (4)	0 14 (10)	0 12 (6)	0.15 (14)	0.38 (48)
Total	99.7	99 6	99 7	100 2	100 3	100 0	100 3
Cations based on 6 oxygens							
Si	1 979	1 992	1 886	1 984	1 998	1 995	1 973
Al	0 007	0 007	0.006	0.008	0 008	0 009	0.022
Mg	1 639	1.624	1.567	1.650	1.646	1.626	1 665
Na	0.001	0.001	0.001	0.001	0.001	0 001	0 003
Ca	0 030	0.026	0 026	0.027	0.020	0 025	0 033
Ti	0 005	0.004	0.004	0.004	0 004	0 005	0 004
Fe	0.332	0 328	0 315	0 313	0 299	0 315	0 283
Mn	0.014	0.015	0.014	0 015	0.014	0 015	0.014
Cr	0 005	0 004	0 003	0 004	0 003	0 004	0 011
Total	4 011	4 001	4 018	4 006	3 993	3 994	4 008
Fe/Mn	23.03	22 13	23 02	21 45	21 00	21 01	19 96
Fe/Mg	0.202	0 202	0 201	0 190	0 182	0 194	0 170

Appendix 4: High-Ca Pyroxenes (wt%)

	H6 Canon City [21]	H6 Chiang Khan [25]	H5 Ucera [24]	H5 Allegan [21]	H4 Farmville [39]	H4 Avanhandava [44]	HH4 Burnwell [21]
SiO2	53 7 (4)	54 5 (5)	53 9 (2)	54.8 (3)	53.7 (9)	54 5 (7)	53 4 (16)
Al2O3	0 76 (4)	0 6 (2)	0.59 (20)	0 51 (11)	1 00 (62)	0 84 (50)	2 40 (185)
MgO	16.7 (3)	17 4 (3)	16 9 (2)	16.9 (2)	18.5 (20)	16.7 (4)	19 6 (26)
Na2O	0 59 (11)	0 53 (5)	0.54 (10)	0 54 (5)	0 53 (10)	0.58 (9)	0 73 (22)
CaO	22 2 (3)	22.4 (4)	22.5 (5)	22 7 (2)	20 2 (29)	22 6 (3)	17 0 (30)
TiO2	0 54 (11)	0 48 (8)	0.49 (3)	0.39 (8)	0 49 (20)	0 50 (23)	0.58 (47)
FeO	3 66 (14)	3 55 (24)	3.52 (24)	3.23 (14)	3 89 (97)	3.20 (17)	4.59 (114)
MnO	0 23 (3)	0 22 (3)	0 23 (4)	0 23 (3)	0.25 (5)	0.22 (3)	0.32 (7)
Cr2O3	0 90 (18)	0 79 (10)	0 78 (7)	0 73 (7)	0.95 (32)	0 94 (39)	1 36 (44)
Total	99 3	100 5	99.4	100 0	99 4	100 1	99 9
Cations based on 6 oxygens							
Si	1 975	1 978	1 978	1 995	1 962	1 983	1 934
Al	0 033	0 026	0 026	0 022	0 043	0 036	0 103
Mg	0.915	0.942	0.925	0.916	1.007	0.905	1 055
Na	0.042	0.037	0.038	0.038	0.037	0 041	0 051
Ca	0.876	0.870	0.884	0.885	0.791	0 882	0 659
Ti	0 015	0 013	0 014	0 011	0 013	0 014	0 016
Fe	0.113	0 108	0 108	0 098	0 119	0.097	0.139
Mn	0.007	0 007	0 007	0 007	0 008	0 007	0.010
Cr	0.026	0 023	0.023	0 021	0 028	0 027	0 039
Total	4 001	4 004	4 003	3 992	4 008	3 992	4 005
Fe/Mn	15.66	15 96	15.10	14.16	15 26	14 19	14.07
Fe/Mg	0 123	0 114	0 117	0 107	0 118	0 108	0 131

Appendix 5: Table 2 – Chemical Parameters for Mineral Phases

Mineral Phase[1]	Defining Criteria[2]
Olivine	Mg: 20-52, Si: 32-53, Ca· 0-3
Low-Ca Pyroxene	Mg: 15-35, Si: 53-72, Ca: 0-4
High-Ca Pyroxene	Mg: 7-20, Si: 47-62, Ca: 15-40, Al: 0-6
Pigeonite	Mg: 12-30, Si. 48-65, Ca: 4-12
FeS	S· 20-70
Kamacite	Fe: 85-101, Ni. 0-10
Taenite	Fe. 50-100, Ni: 10-35
Plagioclase	Al· 12-35, Si: 54-74, Na. 2-7, K: 0-4
Phosphate	P· 10-57, Ca· 25-70
Chromite	Cr· 15-80
Ilmenite	Ti: 20-100
K-rich Phase	Si: 50-80, K: 4-20
SiAl-rich Phase	Si. 40-85, Al: 4-12

Note These criteria, based upon preliminary EDS analyses, apply only to the mineral phases in our H chondrite specimens

1 – The criteria are in terms of percentage of spectrum as provided by the *Feature Scan* software The values are similar to the oxide weight percentages for given elements The seemingly wide ranges allow mineral phases to be appropriately classified even if they partially overlap adjacent phases

2 – The phases are organized according to a first-fit For example, if an analyzed phase does not meet the olivine criteria, *Feature Scan* compares the phase to low-Ca pyroxene If the analyzed phase does not meet the low-Ca pyroxene criteria, it is compared to the next mineral phase on the list in descending order until it finds the first match

Vita

Joshua Chamot was born in Alexandria, Virginia on June 2, 1976 He graduated as a Valedictorian of Lake Braddock Secondary School in 1994 and entered the College of William and Mary in Williamsburg, Virginia in that same year. In 1998, Joshua graduated with departmental honors in Music and Geology and left Virginia to attend the University of Tennessee-Knoxville. En route to a career as a science journalist, Joshua first wanted to complete a thesis in a scientific field. In December of 2000, he received his Master of Science degree in geology from the Univversity of Tennessee. In the time since his enrollment at the University of Tennessee, Joshua has published over thirty articles in several national and international publications He continues to write extensively for several publications including *Geotimes*, published by the American Geological Institute.